J|A|C|S ARTICLES

Published on Web 12/22/2008

The QTAIM Approach to Chemical Bonding Between Transition Metals and Carbocyclic Rings: A Combined Experimental and Theoretical Study of $(\eta^5\text{-}C_5H_5)Mn(CO)_3$, $(\eta^6\text{-}C_6H_6)Cr(CO)_3$, and $(E)\text{-}\{(\eta^5\text{-}C_5H_4)CF{=}CF(\eta^5\text{-}C_5H_4)\}(\eta^5\text{-}C_5H_5)_2Fe_2$

Louis J. Farrugia,*,† Cameron Evans,† Dieter Lentz,‡ and Max Roemer‡

WestCHEM, Department of Chemistry, University of Glasgow, Glasgow G12 8QQ, Scotland, U.K., and Institut für Chemie - Anorganische und Analytische Chemie, Fachbereich Biologie, Chemie, Pharmazie, Freie Universität, D-14195 Berlin, Germany

Received October 22, 2008; E-mail: louis@chem.gla.ac.uk

Abstract: Experimental charge densities for $(C_5H_5)Mn(CO)_3$ (**2**), $(\eta^6\text{-}C_6H_6)Cr(CO)_3$ (**3**), and $(E)\text{-}\{(\eta^5\text{-}C_5H_4)\text{-}CF{=}CF(\eta^5\text{-}C_5H_4)\}(\eta^5\text{-}C_5H_5)_2Fe_2$ (**4**) have been obtained by multipole refinement of high-resolution X-ray diffraction data at 100 K. The resultant densities were analyzed using the quantum theory of atoms in molecules (QTAIM). The electronic structures of these and related π-hydrocarbyl complexes have also been studied by ab initio density functional theory calculations, and a generally good agreement between theory and experiment with respect to the topological parameters was observed. The topological parameters indicate significant metal−ring covalency. A consistent area of disagreement concerns the topology of the metal−ring interactions. It is shown that because of the shared-shell bonding between the metal and the ring carbons, an annulus of very flat density ρ and very small $\nabla\rho$ is formed, which leads to topologically unstable structures close to catastrophe points. This in turn leads to unpredictable numbers of metal−C bond paths for ring sizes greater than four and fewer M−C bond paths than expected on the basis of the formal hapticity. This topological instability is a general feature of metal−π-hydrocarbyl interactions and means that a localized approach based on individual $M-C_{ring}$ bond paths does not provide a definitive picture of the chemical bonding in these systems. However, other QTAIM indicators, such as the virial paths, the delocalization indices, and the source function, clearly demonstrate that for the *n*-hapto $(\eta^n\text{-}C_nH_n)M$ unit, there is generally a very similar level of chemical bonding for all $M-C_{ring}$ interactions, as expected on the basis of chemical experience.

Introduction

The vital importance of π-carbocylic ligands such as $\eta^5\text{-}C_5H_5$ and $\eta^6\text{-}C_6H_6$ in organometallic chemistry hardly needs emphasis,[1] and their bonding to transition metals is very well understood.[2] Despite their familiarity, metallocenes such as ferrocene, $(\eta^5\text{-}C_5H_5)_2Fe$ (**1**), and its derivatives still remain a topic of intense research interest.[1d−g] The eclipsed D_{5h} conformation of **1** is well-established as the ground-state structure in the gas phase[3] and in the crystalline state in the orthorhombic modification,[4] which is the thermodynamically stable form below 242 K. The crystal structure of **1** is complicated by disorder and phase transitions, as summarized by Dunitz[5a] and Brock and Fu.[5b] As recently discussed by Coriani et al.,[6] compounds such as **1** present particular problems in obtaining accurate optimized ab initio geometries. Success is critically dependent on the level of electron correlation used, and recent CCSD(T) calculations by these authors[6] give superb geometrical agreement with experiment and indicate that the eclipsed D_{5h} structure lies 1.15 kcal mol^{-1} lower in energy than the staggered

† University of Glasgow.
‡ Freie Universität Berlin.

(1) (a) Cotton, F. A.; Wilkinson, G. *Advanced Inorganic Chemistry*; Wiley: New York, 1988; Vol. 5. (b) Elschenbroich, C. *Organometallics: A Concise Introduction*; Wiley-VCH: Weinheim, Germany, 2006. (c) Crabtree, R. H. *The Organometallic Chemistry of the Transition Metals*; Wiley-Blackwell: Oxford, U.K., 2005. (d) *Ferrocenes*; Togni, A., Hayashi, T., Eds.; VCH: Weinheim, Germany, 1995. (e) *Metallocenes: Synthesis, Reactivity, Applications*; Togni, A., Halterman, R. L., Eds.; Wiley-VCH: Weinheim, Germany, 1998; Vols. *1* and *2*. (f) Long, N. J. *Metallocenes: An Introduction to Sandwich Complexes*; Blackwell Science Ltd.: Oxford, U.K., 1998. (g) *Metallocenes in Regio- and Stereoselective Synthesis*; Takahashi, T., Hargreaves, A. E., Eds.; Springer-Verlag: Berlin, 2003.

(2) (a) Moffitt, W. *J. Am. Chem. Soc.* **1954**, *76*, 3386. (b) Dunitz, J. D.; Orgel, L. E. *J. Chem. Phys.* **1955**, *23*, 954. (c) Elian, M.; Chen, M. M. L.; Mingos, D. M. P.; Hoffmann, R. *Inorg. Chem.* **1976**, *15*, 1148. (d) Clack, D. W.; Warren, K. D. *Struct. Bonding (Berlin)* **1980**, *39*, 1. (e) Weber, J.; Goursot, A.; Pénigault, E.; Ammeter, J. H.; Bachmann, J. *J. Am. Chem. Soc.* **1982**, *104*, 1491. (f) Xu, Z.-F.; Xie, Y.; Feng, W.-L.; Schaefer, H. F. *J. Phys. Chem. A.* **2003**, *107*, 2716, and references therein. (g) Yamaguchi, Y.; Ding, W.; Sanderson, C. T.; Borden, M. L.; Morgan, M. J.; Kutal, C. *Coord. Chem. Rev.* **2007**, *251*, 515. (h) Boccia, A.; Marrani, A. G.; Stranges, S.; Zanoni, R.; Alagia, M.; Cossi, M.; Iozzi, M. F. *J. Chem. Phys.* **2008**, *128*, 154315.

(3) Bohn, R. K.; Haaland, A. *J. Organomet. Chem.* **1966**, *5*, 470.

(4) Seiler, P.; Dunitz, J. D. *Acta Crystallogr., Sect. B* **1982**, *38*, 1741.

(5) (a) Dunitz, J. D. *Acta Crystallogr., Sect. B* **1995**, *51*, 619. (b) Brock, C. P.; Fu, Y. *Acta Crystallogr., Sect. B* **1997**, *53*, 928.

(6) Coriani, S.; Haaland, A.; Helgaker, T.; Jørgensen, P. *ChemPhysChem* **2006**, *7*, 245.

D_{5d} conformation. In view of such tiny energy differences, it is not surprising that the actual structure adopted by **1** in the crystalline phase depends on kinetic as well as thermodynamic factors.[5a] This is borne out by an examination of structures in the Cambridge Structural Database[7] where **1** is included as a guest in the lattice and where examples of staggered,[8] eclipsed,[9] and "in-between" ring geometries[10] in **1** may be found.

While the electronic structures of **1** and related molecules have been intensely investigated using orbital analysis,[2,6] the study of their bonding by an alternative density-based approach, Bader's quantum theory of atoms in molecules (QTAIM),[11] is less well developed. The central importance of the bond path [and associated bond critical points (bcp's) and interatomic surface] in the QTAIM has been asserted by Bader.[12] It results in a rigorous definition of chemical structure and allows a distinction between chemical *bonds* and chemical *bonding*, a distinction which has been the subject of considerable heat in the literature.[13] A recent interpretation of the bond path (bp) by Pendás et al.[14] in terms of a preferred pathway of quantum-mechanical exchange may allow for a more considered approach. Cortés-Guzmán and Bader,[15] Lyssenko et al.,[16] and Zhang et al.[17] have presented theoretical topological analyses of the D_{5d} and D_{5h} conformations of **1** using the density functional theory (DFT) approach with the B3LYP functional. Both conformations give essentially identical topologies, with five bond paths between the Fe atom and the individual C atoms in the η^5-C_5H_5 ring. This leads to a ring of five bcp's, which is interspersed with a ring of five ring critical points (rcp's). All 10 cp's lie approximately in a plane parallel to the C_5 plane, and the rcp's have charge densities nearly identical to those of the bcp's. Another rcp and an associated cage cp (ccp) are derived from the C_5 ring, and we designate this the [5, 5, 1 + 1] topology. This topological constellation has at its heart the seeds of ambiguity. The presence of bcp's and rcp's in close proximity and with almost identical charge densities presages a catastrophe situation, specifically, the fold catastrophe described by Bader,[11] whereby an rcp and a bcp coalesce into a singularity and the ring structure is lost. The topological structure is thus unstable, and small perturbations in the charge density (arising, for instance, from small nuclear displacements) can lead to a catastrophe situation and a change in the chemical topology.[18] In one theoretical QTAIM study on (η^5-C_5H_5)$(CO)_2$-Mn(η^2-$HSiCl_3$),[19] the same [5, 5, 1 + 1] topology between the Mn atom and the η^5-C_5H_5 ring as described above was observed, while for (η^5-C_5H_5)Ti(C_7H_9),[20] only four bond paths between the Ti and the (η^5-C_5H_5) ring were found. This situation led Bader and Matta[19,20] to conclude that "the bonding... is not well represented in terms of individual atomic interactions" and that the metal−ring interaction is best described as involving "the delocalized density of the entire ring perimeter". This delocalized QTAIM view of the metal−ring chemical bonding in M(η^5-C_5H_5) (and related) units is clearly a pertinent one and is developed in this article. Moreover, it is consistent with the known, very low barrier for rotation of the η^5-C_5H_5 ring.[21]

Despite the central importance of η^n-carbocyclic ligands in organometallic chemistry, there have been relatively few experimental charge density studies using QTAIM that examine this essential metal−ligand interaction. Macchi et al.[22] have reported such a study of the 1,5-cyclooctadiene complex Ni(η^4-C_8H_{12})$_2$, which rationalized the metal−olefin topology in terms of the classical Dewar−Chatt−Duncanson[23] (DCD) model. The inward curvatures of the Ni−C bond paths for the two independent Ni−(η^2-C_2) interactions were interpreted as being consistent with the DCD model. More recently, Scherer et al.[24] have argued that the experimental and theoretical bond path topologies in Ni(η^2-C_2H_4)(dbpe) are more complex. They suggest that the charge polarizations at the metal atom provide

(7) Allen, F. R. *Acta Crystallogr., Sect. B* **2002**, *58*, 380.
(8) (a) Haneline, M. R.; Gabbai, F. P. *Angew. Chem., Int. Ed.* **2004**, *43*, 5471. (b) Tikhonova, I. A.; Dolgushin, F. M.; Tugashov, K. I.; Petrovskii, P. V.; Antipin, M. Yu.; Shur, V. B. *Izv. Akad. Nauk SSSR, Ser. Khim.* **2004**, 2754. (c) Day, M. W.; Matxger, A. J.; Grubbs, R. H. Reference code OCUJIF in the Cambridge Stuctural Database, submitted as a private communication, 2001. (d) Odagaki, Y.; Hirotsu, K.; Higuchi, T.; Harada, A.; Takahashi, S. *J. Chem. Soc., Perkin Trans. 1* **1990**, 1230. (e) Kabir, S. E.; Rahman, A. F. M. M.; Parvin, J.; Malik, K. M. A. *Indian J. Chem., Sect. A* **2003**, *43*, 2518.
(9) (a) Muller, M.; Edwards, A. J.; Prout, K.; Simpson, W. M.; Heyes, S. J. *Chem. Mater.* **2000**, *12*, 1314. (b) Atencio, R.; Domasevitch, K. V.; Zaworotko, M. J. *Cryst. Eng.* **2000**, *3*, 63. (c) Razak, I. A.; Fun, H.-K.; Yamin, B. M.; Boshaala, A. M. A.; Chinnakali, K. *Acta Crystallogr., Sect. C* **1998**, *54*, 912. (d) Olmstead, M. M.; Hao, L.; Balch, A. L. *J. Organomet. Chem.* **1999**, *578*, 85. (e) Crane, J. D.; Hitchcock, P. B.; Kroto, H. W.; Taylor, R.; Walton, D. R. M. *J. Chem. Soc., Chem. Commun.* **1992**, 1764.
(10) (a) O'Connor, A. R.; Nataro, C.; Golen, J. A.; Rheingold, A. L. *J. Organomet. Chem.* **2004**, *689*, 2411. (b) Paine, K. T.; Weyhermuller, T.; Bothe, E.; Wieghardt, K.; Chaudhuri, P. *Dalton Trans.* **2003**, 3136.
(11) (a) Bader, R. F. W. *Atoms in Molecules: A Quantum Theory*; International Series of Monographs in Chemistry, Vol. 2; Oxford University Press: Oxford, U.K., 1990. (b) Popelier, P. *Atoms in Molecules: An Introduction*; Prentice Hall: Harlow, U.K., 2000. (c) *The Quantum Theory of Atoms in Molecules: From Solid State to DNA and Drug Design*; Matta, C. F., Boyd, R. J., Eds.; Wiley-VCH: Weinheim, Germany, 2007.
(12) Bader, R. F. W. *J. Phys. Chem. A* **1998**, *102*, 7314.
(13) (a) Abramov, Y. A. *J. Phys. Chem. A* **1997**, *101*, 5725. (b) Haaland, A.; Shorokhov, D. J.; Tverdova, N. J. *Chem.—Eur. J.* **2004**, *10*, 4416. (c) Cioslowski, J.; Mixon, S. T.; Edwards, W. D. *J. Am. Chem. Soc.* **1991**, *113*, 1083. (d) Cioslowski, J.; Mixon, S. T. *Can. J. Chem.* **1992**, *70*, 443. (e) Cioslowski, J.; Mixon, S. T. *J. Am. Chem. Soc.* **1992**, *114*, 4382. (f) Cioslowski, J.; Edgington, L.; Stefanov, B. B. *J. Am. Chem. Soc.* **1995**, *117*, 10381. (g) Bader, R. F. W.; Fang, D.-C. *J. Chem. Theory Comput.* **2005**, *1*, 403. (h) Matta, F.; Hernández-Trujillo, J.; Tang, T.-H.; Bader, R. F. W. *Chem.—Eur. J.* **2003**, *9*, 1940. (i) Poater, J.; Solà, M.; Bickelhaupt, F. M. *Chem.—Eur. J.* **2006**, *12*, 2889. (j) Bader, R. F. W. *Chem.—Eur. J.* **2006**, *12*, 2896. (k) Poater, J.; Solà, M.; Bickelhaupt, F. M. *Chem.—Eur. J.* **2006**, *12*, 2902.
(14) Pendás, M. A.; Francisco, E.; Blanco, M. A.; Gatti, C. *Chem.—Eur. J.* **2007**, *13*, 9362.
(15) Cortés-Guzmán, F.; Bader, R. F. W. *Coord. Chem. Rev.* **2005**, *249*, 633.
(16) Lyssenko, K. A.; Golovanov, D. G.; Antipin, M. Yu. *Mendeleev Commun.* **2003**, *13*, 209.
(17) Zhang, G.; Zhang, H.; Sun, M.; Liu, Y.; Pang, X.; Yu, X.; Liu, B.; Li, Z. *J. Comput. Chem.* **2007**, *28*, 2260.
(18) This situation has already been reached for the ferrocene molecule, since Lyssenko et al.[16] and Zhang et al.[17] have reported that the rcp associated with the C_5 ring and the cage cp were coalesced and not detected, giving the [5, 5] topology, whereas they were present but very close in the study by Cortés-Guzmán and Bader.[15]
(19) Bader, R. F. W.; Matta, C. F. *Organometallics* **2004**, *23*, 6253.
(20) Bader, R. F. W.; Matta, C. F. *Inorg. Chem.* **2001**, *40*, 5603.
(21) Albright, T. A.; Hofmann, P.; Hoffmann, R. *J. Am. Chem. Soc.* **1977**, *99*, 7546, and references therein.
(22) Macchi, P.; Proserpio, D. M.; Sironi, A. *J. Am. Chem. Soc.* **1998**, *120*, 1447.
(23) (a) Dewar, J. S. *Bull. Soc. Chim. Fr.* **1951**, *18*, C71. (b) Chatt, J.; Duncanson, L. A. *J. Chem. Soc.* **1953**, 2939.
(24) Scherer, W.; Eickerling, G.; Shorokhov, D.; Gullo, E.; McGrady, G. S.; Sirch, P. *New J. Chem.* **2006**, *30*, 309.
(25) (a) Hebben, N.; Himeel, H.-J.; Eickerling, G.; Herrmann, C.; Reiher, M.; Herz, V.; Presnitz, M.; Schere, W. *Chem.—Eur. J.* **2007**, *13*, 10078. (b) Reisinger, A.; Trapp, N.; Krossing, I.; Altmannshofer, S.; Herz, V.; Presnitz, M.; Scherer, W. *Angew. Chem., Int. Ed.* **2007**, *46*, 8295. (c) Knapp, A.; Frenking, G. *Angew. Chem., Int. Ed.* **2008**, *47*, 7796. (d) Himmel, D.; Trapp, N.; Krossing, I.; Altmannshofer, S.; Herz, V.; Eickerling, G.; Scherer, W. *Angew. Chem., Int. Ed.* **2008**, *47*, 7798.

a less ambiguous indicator of the extent of σ donation and π back-donation, and similar considerations apply to other homoleptic alkene[25a] and alkyne[25b−d] complexes. In the pentadienyl complex Zr(η^5-2,4-C_7H_{11})($NMe_2CHPhCH_2CMe$=CHC-Me=CH_2), the formal Zr−η^5-pentadienyl interaction results in only a single Zr−C bond path, connecting to the central C atom with the shortest Zr−C distance.[26] A few experimental topological studies on metal cyclopentadienyl complexes have appeared recently.[27] Borissova et al.[28] and Van der Maelen et al.[29] both reported the [5, 5, 1 + 1] topology for each ring in their respective studies on (η^5-C_5H_5)$_2$Ru and (η^5-C_5Me_5)$_2$Zn$_2$. However, Lecomte and co-workers[30] reported only three Mn−C bp's for the formal Mn−η^5 interaction in (η^5-C_5H_4Me)$(CO)_2$Mn{η^2-O=C=C[(μ-η^2-C≡CPh)$Co_2(CO)_6$]Ph}, and a similar situation was observed by Scherer el al.[31] in (η^5-C_5H_4Me)$(CO)_2$Mn(η^2-$HSiPh_2F$). Moreover, in the borylene complex{(η^5-C_5H_5)$(CO)_2$-Mn}$_2$(μ-BBu^t), Stalke and co-workers[32] found from the experimental density only two Mn−C bond paths in each of the independent (η^5-C_5H_5)Mn units, though five Mn−C bond paths were obtained by theory. While the topology of the metal−cyclopentadienyl interaction was not the central focus in any of these studies, it is clear that the experimental evidence is conflicting.

In 2006, we reported[33] a topological charge density study of the trimethylenemethane complex Fe{$C(CH_2)_3$}$(CO)_3$, where ambiguities arose in the QTAIM interpretation of the interaction between the Fe atom and the hydrocarbyl ligand. Herein we present experimental and theoretical charge density studies of the well-known complexes (η^5-C_5H_5)$Mn(CO)_3$ (**2**) and (η^6-C_6H_6)$Cr(CO)_3$ (**3**), as representative models for half-sandwich compounds, and of (*E*)-{(η^5-C_5H_4)CF=CF(η^5-C_5H_4)}(η^5-C_5H_5)$_2$-Fe_2 (**4**),[34] a model for ferrocene (for which an experimental study is not practical). These studies raise similar issues and provide compelling experimental evidence that a localized QTAIM approach focusing solely on individual metal−C_{ring} bond paths does not provide a complete understanding of the metal−η^n-carbocyclic ligand interactions. We show that other topological indicators, particularly the delocalization indices $\delta(\Omega_A, \Omega_B)$ and the integrated source function, are better guides in the QTAIM interpretation of this chemical interaction.

Experimental Section

Data Collection, Processing, and Spherical Atom Refinement. Crystals of **2** and **3** were obtained by sublimation of the commercial products (Aldrich), while crystals of **4** were obtained by recrystallization from dichloromethane. Details of the data collection procedures are given in Table 1. Single crystals of suitable size were attached to a glass fiber with silicone grease and cooled from ambient temperature to 100 K over a period of 1 h using an Oxford Instruments Cryostream. Data were collected using ω- and φ-oscillation scans of ∼2.0° on a Nonius KappaCCD diffractometer running under Collect software.[35] The images were integrated and precise unit cell dimensions and errors determined by postrefinement of the setting angles of the reflections using the Denzo integration software,[36] as described elsewhere.[33] Absorption corrections by Gaussian quadrature,[37] based on the measured crystal faces, were applied to the reflection data. The data were then scaled, and a semiempirical correction[38] (without a θ-dependent correction) was applied using the program SADABS[39] to remove any residual absorption anisotropy due to the mounting medium and to account for other instrumental instabilities. Typical correction factors were in range 0.7−0.9. Data were then sorted and merged with SORTAV,[40] giving mean redundancies of 14.0, 16.5, and 32.5 for **2**, **3**, and **4**, respectively. Spherical atom refinements with SHELXL97-2[41] were initially undertaken using full-matrix least-squares on F^2 and all of the unique data. All of the non-H atoms were allowed anisotropic thermal motion. Details of this refinement are given in Table 1. Thermal ellipsoid plots were obtained using the program ORTEP-3 for Windows.[42] All of the calculations were carried out using the WinGX package[43] of crystallographic programs. Because of the difficulty of obtaining accurate integrated intensities using Denzo when the $k_{\alpha1}/k_{\alpha2}$ splitting becomes too great (i.e., $\theta \gtrsim 50°$), the data sets for multipole refinements were truncated at $(\sin\theta)/\lambda \leq 1.078$ Å^{-1} ($\theta_{max} = 50°$). All of the data sets were 100% complete to this resolution limit.

Multipole Refinement. The multipole formalism of Hansen and Coppens[44] as implemented in the XD-2006 program suite[45] was used. The aspherical atomic electron density $\rho(\mathbf{r})$ as a function of position $\mathbf{r}$ is given by

$$\rho(\mathbf{r}) = \rho_c(\mathbf{r}) + P_v\kappa^3\rho_v(\mathbf{r}) + \rho_d(\kappa'\mathbf{r}) \quad (1)$$

where ρ_c and ρ_v are the core and spherical valence densities, respectively, and

$$\rho_d(\kappa'\mathbf{r}) = \sum_{l=0}\kappa^3 R_l(\kappa'\mathbf{r})\sum_{m=0}^{l} P_{lm\pm}y_{lm\pm}(\mathbf{r}/r) \quad (2)$$

(26) Pillet, S.; Wu, G.; Kulsomphob, V.; Harvey, B. J.; Ernst, R. D.; Coppens, P. *J. Am. Chem. Soc.* **2003**, *125*, 1937.

(27) There have also been a number of "classic" experimental charge density studies on transition-metal−π-carbocyclic complexes using analysis of the deformation densities rather than QTAIM. See: (a) Rees, B.; Coppens, P. *Acta Crystallogr., Sect. B* **1973**, *29*, 2515. (b) Wang, Y.; Coppens, P. *Inorg. Chem.* **1976**, *15*, 1122. (c) Mitschler, A.; Rees, B.; Lehmann, M. S. *J. Am. Chem. Soc.* **1978**, *100*, 3390. (d) Angermund, K.; Claus, K. H.; Goddard, R.; Kruger, C. *Angew. Chem., Int. Ed. Engl.* **1985**, *24*, 237. (e) Wang, Y.; Angermund, K.; Goddard, R.; Krüger, C. *J. Am. Chem. Soc.* **1987**, *109*, 587. (f) Antipin, M. Yu.; Lyssenko, K. A.; Boese, R. *J. Organomet. Chem.* **1996**, *508*, 259. (g) Lyssenko, K. A.; Antipin, M. Yu.; Ketkov, S. Yu. *Russ Chem. Bull., Int. Ed.* **2001**, *50*, 130. There is also a topological study of a Zr−indenyl complex that shows a single Zr−C bond path to the C_5 ring, as a result of the significant ring slippage. See: (h) Stash, A. I.; Tanaka, K.; Shiozawa, K.; Makino, H.; Tsirelson, V. G. *Acta Crystallogr., Sect. B* **2005**, *61*, 418.

(28) Borissova, A. O.; Antipin, M. Yu.; Perakalin, D. S.; Lyssenko, K. A. *CrystEngComm* **2008**, *10*, 827.

(29) Van der Maelen, J. F.; Gutiérrez-Puebla, E.; Monge, Á.; García-Granda, S.; Resa, I.; Carmona, E.; Fernández-Diaz, M. T.; McIntyre, G. J.; Pattison, P.; Weber, H.-P. *Acta Crystallogr., Sect. B* **2007**, *63*, 862.

(30) Ortin, Y.; Lugan, N.; Pillet, S.; Souhassou, M.; Lecomte, C.; Costuas, K.; Saillard, J.-Y. *Inorg. Chem.* **2005**, *44*, 9607.

(31) Scherer, W.; Eickerling, G.; Tafipolsky, M.; McGrady, G. S.; Sirch, P.; Chatterton, N. P. *Chem. Commun.* **2006**, 2986.

(32) Flierler, U.; Burzler, M.; Leusser, D.; Henn, J.; Ott, H.; Braunschweig, H.; Stalke, D. *Angew. Chem., Int. Ed.* **2008**, *47*, 4321.

(33) Farrugia, L. J.; Evans, C.; Tegel, M. *J. Phys. Chem. A* **2006**, *110*, 7052.

(34) Roemer, M.; Lentz, D. *Eur. J. Inorg. Chem.* **2008**, 4875.

(35) *Collect Data Collection Software*; Nonius B.V.: Delft, The Netherlands, 1999.

(36) (a) Otwinowski, Z.; Minor, W. *Methods Enzymol.* **1997**, *276*, 307. (b) Otwinowski, Z.; Minor, W. *International Tables for Crystallography*, 1st online ed.; Springer: Heidelberg, Germany, 2006; Vol. F, Chapter 11.4, p 226−235.

(37) Coppens, P.; Leiserowitz, L.; Rabinovich, D. *Acta Crystallogr.* **1965**, *18*, 1035.

(38) Blessing, R. H. *Acta Crystallogr., Sect. A* **1995**, *51*, 33.

(39) Sheldrick, G. M. *SADABS*, version 2008/1; University of Göttingen: Göttingen, Germany, 2008.

(40) Blessing, R. H. *J. Appl. Crystallogr.* **1997**, *30*, 421.

(41) Sheldrick, G. M. *Acta Crystallogr., Sect. A* **2008**, *64*, 112.

(42) Farrugia, L. J. *J. Appl. Crystallogr.* **1997**, *30*, 565.

(43) Farrugia, L. J. *J. Appl. Crystallogr.* **1999**, *32*, 837.

(44) Hansen, N. K.; Coppens, P. *Acta Crystallogr., Sect. A* **1978**, *34*, 909.

(45) Volkov, A.; Macchi, P.; Farrugia, L. J.; Gatti, C.; Mallinson, P.; Richter, T.; Koritsanszky, T. *XD 2006: A Computer Program for Multipole Refinement, Topological Analysis of Charge Densities and Evaluation of Intermolecular Interaction Energies From Experimental or Theoretical Structure Factors*, 2006.

Table 1. Experimental Crystallographic Details

	2	**3**	**4**
		Data Collection	
formula	$C_8H_5MnO_3$	$C_9H_6CrO_3$	$C_{22}H_{18}F_2Fe_2$
color	yellow	yellow	red
M_r	204.06	214.14	432.06
space group	$P2_1/n$	$P2_1/m$	$P4_2/n$
crystal system	monoclinic	monoclinic	tetragonal
a (Å)	10.7573(3)	6.0230(2)	16.9812(4)
b (Å)	6.9348(2)	10.9397(2)	16.9812(4)
c (Å)	11.6614(3)	6.5172(1)	5.8607(1)
β (deg)	115.764(1)	100.728(1)	90
V (Å^{-3})	783.46(4)	421.912(17)	1690.00(6)
Z	4	2	4
D_{calcd} (g cm^{-3})	1.73	1.69	1.70
$F(000)$	408	216	880
λ (Å)	0.71073	0.71073	0.71073
μ(Mo Kα) (mm^{-1})	1.64	1.32	1.739
crystal size (mm)	0.25 × 0.20 × 0.15	0.45 × 0.34 × 0.23	0.43 × 0.29 × 0.23
transmission coefficient range	0.617−0.815	0.601−0.752	0.434−0.706
θ range (deg)	2.15−50.06	3.18−55.41	2.4-−50.03
no. of data used for merging	115084	91696	289758
no. of unique data	8240	5616	8904
h range	−23 to 23	−13 to 13	−36 to 36
k range	−14 to 14	−25 to 25	−36 to 34
l range	−25 to 25	−14 to 14	−12 to 12
R_{int}[a]	2.86	2.80	3.53
R_σ[a]	1.44	1.11	2/58
		Spherical Atom Refinement	
no. of data in refinement	8240	5616	8904
no. of refined parameters	115	68	127
final R [$I > 2\sigma(I)$] (all data)[a]	2.36 (3.03)	1.91 (1.98)	2.52 (3.0)
R_w^2 [$I > 2\sigma(I)$] (all data)[a]	6.52 (6.75)	6.00 (6.05)	6.59 (6.76)
goodness of fit	1.041	0.946	1.092
electron density residuals (e Å^{-3})	0.628, −0.729	0.741, −0.948	1.293, −0.62
max shift (esd) in last cycle	10^{-3}	10^{-3}	5.0×10^{-3}
		Multipole Refinement	
no. of data in refinement	7245	4506	8252
no. of refined parameters (last cycle)	334	195	252
final R [$F > 3\sigma(F)$] (all data)[a]	1.60 (2.48)	0.84 (1.10)	1.78 (2.28)
R_w [$F > 3\sigma(F)$][a]	1.20	1.0	1.58
goodness of fit	1.429	1.662	1.401
electron density residuals (all data) (e Å^{-3})	0.281, −0.257 (0.051 rms)	0.197, −0.175, (0.028 rms)	0.501, −0.445 (0.059 rms)
electron density residuals (truncated data[b]) /eÅ^{-3}	0.140, −0.106 (0.027 rms)	0.113, −0.121 (0.019 rms)	0.323, −0.215 (0.035 rms)
max shift (esd) in last cycle	3.0×10^{-5}	10^{-5}	2.0×10^{-5}

[a] $R = \sum(|F_o| - |F_c|)/\sum F_o$; $R_w = \{\sum w(F_o - F_c)^2/\sum w(F_o)^2)\}^{1/2}$; $R_w^2 = \{\sum w(F_o^2 - F_c^2)^2/\sum w(F_o^2)^2\}^{1/2}$; $R_\sigma = \sum\sigma(F_o^2)/\sum F_o^2$; $R_{int} = \sum\{n/(n-1)\}^{1/2}|F_o^2 - F_o^2(\text{mean})|/\sum F_o^2$, where the summation is carried out only when more than one symmetry equivalent is averaged. [b] Truncated at (sin θ)/$\lambda \leq 0.8$ Å^{-1}.

is the term accounting for the deformation valence densities. The $y_{lm\pm}$ are density-normalized real spherical harmonics, P_v and $P_{lm\pm}$ are the refinable populations, and κ and κ' are spherical and valence deformation expansion−contraction parameters, respectively. The function minimized in the least-squares procedure was $\sum w(|F_o| - k|F_c|)^2$, where only those reflections with $F > 3\sigma(F)$ were included in the refinement and the weights w were taken as $1/\sigma^2(F)$. The multipole expansion was truncated at the hexadecapole level for the transition-metal atoms, at the octupole level for the F, O, and C atoms, and at the quadrupole level for the H atoms. For all of the complexes, the local coordinate system for the metal-based multipoles was defined with the z axis coincident with the symmetry axis of the M(η^n-C_nH_n) unit. In the initial stages of refinement, contraints were applied to chemically equivalent atoms. For **2** and **3**, these were later released, and the unconstrained refinement was judged satisfactory. For **4**, the unconstrained refinement gave marginally lower residuals but less satisfactory topological properties (in particular, only three Fe−C_{ring} bcp's were observed), so the chemical constraints were retained in the final refinements. The hydrogen positional parameters in **2** and **4** were fixed at the C−H distances determined from the theoretical optimized geometries (1.079 and 1.076 Å respectively), while for **3**, the previously neutron-determined[27a] H atom positional parameters were utilized. Several authors have recently emphasized the importance of employing anisotropic displacement parameters (adp's) for H atoms in multipole refinements.[46] For complex **3**, the previously neutron-determined[27a] H atom adp's were used and scaled according the procedure of Blessing.[47] Since neutron diffraction data were not available, the H atom adp's for **2** and **4** were estimated by the method of Madsen[48] using the SHADE2 web server.[49] These were subsequently kept fixed in all of the refinements. The SHADE2 program has recently been shown[50] to provide an excellent approximation to the H atom adp.

(46) (a) Whitten, A. E.; Spackman, M. A. *Acta. Crystallogr., Sect. B* **2006**, *62*, 875. (b) Whitten, A. E.; Turner, P.; Klooster, W. T.; Piltz, R. O.; Spackman, M. A. *J. Phys. Chem. A.* **2006**, *110*, 8763. (c) Madsen, A. Ø.; Sørensen, H. S.; Flensburg, C.; Stewart, R. F.; Larsen, S. *Acta Crystallogr., Sect. A* **2004**, *60*, 550.
(47) Blessing, R. *Acta Crystallogr., Sect. B* **1995**, *51*, 816.
(48) Madsen, A. Ø. *J. Appl. Crystallogr.* **2006**, *39*, 757.
(49) SHADE2 server: http://shade.ki.ku.dk/docs/index.html.
(50) Munshi, P.; Madsen, A. Ø.; Spackman, M. A.; Larsen, S.; Destro, R. *Acta Crystallogr., Sect. A* **2008**, *64*, 465.

Table 2. Bond Critical Point Properties for Complex **2**[a]

bond	d_1[b]	d_2[b]	$\rho(\mathbf{r}_{bcp})$[c]	$\nabla^2\rho(\mathbf{r}_{bcp})$[d]	λ_1[d]	λ_2[d]	λ_3[d]	ε	$G(\mathbf{r}_{bcp})$[e]	$G(\mathbf{r}_{bcp})/\rho(\mathbf{r}_{bcp})$	$V(\mathbf{r}_{bcp})$[e]	$\lvert V(\mathbf{r}_{bcp})\rvert/G(\mathbf{r}_{bcp})$	$H(\mathbf{r}_{bcp})$[e]
Mn1−C1	0.8940	0.9116	0.95	15.05	−4.32	−4.02	23.39	0.07	1.45	1.51	−1.84	1.27	−0.39
	0.8888	*0.9137*	*0.97*	*12.77*	*−3.95*	*−3.59*	*20.31*	*0.10*	*1.29*	*1.32*	*−1.68*	*1.27*	*−0.39*
Mn1−C2	0.8810	0.9138	0.96	15.0	−4.27	−4.17	23.44	0.02	1.45	1.51	−1.84	1.27	−0.40
	0.8876	*0.9127*	*0.98*	*12.80*	*−3.95*	*−3.64*	*20.39*	*0.08*	*1.29*	*1.32*	*−1.69*	*1.31*	*−0.40*
Mn1−C3	0.8918	0.9085	0.98	14.83	−4.49	−4.39	23.70	0.02	1.47	1.50	−1.91	1.30	−0.43
	0.8883	*0.9135*	*0.98*	*12.71*	*−3.98*	*−3.65*	*20.33*	*0.09*	*1.28*	*1.31*	*−1.68*	*1.31*	*−0.39*
Mn1−C4	1.0745	1.0957	0.47	6.20	−1.45	−0.29	7.94	4.04	0.52	1.10	−0.59	1.13	−0.08
	1.0864	*1.1349*	*0.44*	*5.27*	*−1.41*	*−0.16*	*6.84*	*7.93*	*0.45*	*1.02*	*−0.53*	*1.17*	*−0.08*
Mn1−C5	1.0845	1.1021	0.47	6.14	−1.37	−0.02	7.53	89.5	0.51	1.10	−0.59	1.15	−0.08
	1.0849	*1.1214*	*0.45*	*5.55*	*−1.40*	*−0.35*	*6.97*	*3.00*	*0.45*	*1.01*	*−0.53*	*1.18*	*−0.08*
Mn1−C6	1.0776	1.0880	0.48	6.16	−1.46	−0.35	7.96	3.13	0.52	1.09	−0.61	1.17	−0.09
	1.0875	*1.1143*	*0.45*	*5.13*	*−1.37*	*−0.46*	*6.98*	*1.90*	*0.45*	*0.99*	*−0.53*	*1.18*	*−0.09*
Mn1−C8	1.0797	1.0835	0.46	6.01	−1.28	−0.17	7.45	6.49	0.50	1.09	−0.58	1.16	−0.08
	1.0886	*1.1125*	*0.45*	*5.09*	*−1.36*	*−0.52*	*6.96*	*1.64*	*0.44*	*0.98*	*−0.53*	*1.20*	*−0.09*
C4−C5	0.7142	0.7195	1.97	−13.82	−14.55	−11.97	12.70	0.22	1.84	0.94	−4.66	2.53	−2.81
	0.7174	*0.7188*	*1.92*	*−16.89*	*−14.34*	*−12.11*	*9.56*	*0.18*	*0.60*	*0.31*	*−2.38*	*3.97*	*−1.78*
C5−C6	0.7009	0.7162	2.02	−14.90	−15.45	−12.09	12.64	0.28	1.91	0.94	−4.86	2.54	−2.95
	0.7099	*0.7122*	*1.97*	*−17.87*	*−14.92*	*−12.36*	*9.41*	*0.21*	*0.64*	*0.32*	*−2.53*	*3.95*	*−1.89*
C6−C7	0.6853	0.7428	1.98	−13.87	−15.10	−11.42	12.64	0.32	1.87	0.94	−4.70	2.51	−2.84
	0.7135	*0.7187*	*1.94*	*−17.17*	*−14.51*	*−12.19*	*9.52*	*0.19*	*0.61*	*0.32*	*−2.42*	*3.97*	*−1.81*
C7−C8	0.6966	0.7291	2.03	−15.81	−15.70	−12.52	12.40	0.25	1.88	0.93	−4.86	2.58	−2.98
	0.7117	*0.7178*	*1.95*	*−17.36*	*−14.62*	*−12.23*	*9.9*	*0.19*	*0.62*	*0.32*	*−2.45*	*3.95*	*−1.83*
C8−C4	0.7020	0.7185	2.04	−15.91	−15.78	−12.57	12.43	0.26	1.90	0.93	−4.91	2.58	−3.01
	0.7095	*0.7141*	*1.97*	*−17.77*	*−14.86*	*−12.34*	*9.43*	*0.20*	*0.64*	*0.32*	*−2.52*	*3.94*	*−1.88*
C−O (ave)	0.397	0.757	3.32	−15.6	−34.24	−33.83	53.76	0.01	5.27	1.59	−11.55	2.19	−6.27
	0.403	*0.770*	*3.05*	*−3.9*	*−31.39*	*−31.33*	*58.83*	*0.0*	*5.34*	*1.75*	*−10.96*	*2.05*	*−5.62*
C−H (ave)	0.353	0.723	1.90	−19.8	−19.7	−18.7	18.6	0.06	1.4	0.76	−4.2	3.0	−2.9
	0.385	*0.689*	*1.99*	*−27.2*	*−20.2*	*−19.8*	*12.8*	*0.02*	*0.25*	*0.13*	*−2.4*	*9.6*	*−2.2*

[a] For each compound, values in the first line are from experiment and those in the second line from the gas-phase DFT wave function. [b] d_1 and d_2 are the distances (Å) of the bcp to the nuclei. [c] Units of e Å^{-3}. [d] Units of e Å^{-5}. [e] Units of hartree Å^{-3}.

Each pseudoatom was assigned a neutral-atom core and spherical-valence scattering factor derived from the relativistic Dirac−Fock wave functions of Su and Coppens[51] expanded in terms of the single-ζ functions of Bunge, Barrientos, and Bunge.[52] The valence deformation functions for all atoms apart from the transition metals used a single-ζ Slater-type radial function multiplied by the density-normalized spherical harmonics. The radial fits for the spherical and deformation valence densities of chemically distinct atoms were optimized by refinement of their respective expansion−contraction parameters κ and κ'. Chemically unique atom types were assigned individual κ and κ' parameters. For all atoms apart from the transition metals, a single κ' parameter was used for all of the valence deformation multipoles. For the transition metals, individual κ' parameters for $l = 0$, 4 were used, but with the constraint that $\kappa'_0 = \kappa'_1 = \kappa'_3$. The radial terms used for the transition-metal atoms were either simple Slater functions or the relevant-order Fourier−Bessel transforms of the Su and Coppens[51] wave functions. The 3d transition metals present special problems[53] when modeling the deformation density because of the significantly different radial extensions of the 3d and 4s valence orbitals. The 4s scattering is only significant in the low-angle data, which often suffer most seriously from systematic errors such as extinction and absorption, leading to difficulties in obtaining reliable estimates of the 4s population. Examination of a number of models showed the default treatment of the transition metals in the XD program (which assumes the 4s population to be part of the "core" density population $\rho_c(\mathbf{r})$ and not refined) to be the best treatment for all of the complexes.

Isotropic secondary extinction corrections according to the Becker−Coppens formalism[54] (type-I, Lorentzian distribution of mosaic spread) were applied to all of the data sets. The rigid-bond criterion of Hirshfeld[55] was examined for covalent bonds involving non-H atoms and used to gauge the efficacy of the multipole refinements. For the light-atom−light-atom bonds, all of the Δ(msda) (msda = mean square displacement amplitude) values were less than 1.0×10^{-3} Å^2. The largest values for the covalent bonds involved the metal atom−ring bonds, as expected given the very low barrier for rotation of the ring about the symmetry axis. Typical Δ(msda) values for these bonds were $(1.7-2.2) \times 10^{-3}$ Å^2, while for the M−C(carbonyl) bonds, mean values were 0.9×10^{-3} Å^2. Exploratory refinements using anharmonic thermal parameters for the metal atoms gave no significant improvements, so these were not considered further.

The kinetic energy densities $G(\mathbf{r})$ at the bcp's that are given in Tables 2−4 were estimated using the approximation of Abramov,[56]

$$G(\mathbf{r}) = \frac{3}{10}(3\pi^2)^{2/3}\rho(\mathbf{r})^{5/3} + \frac{1}{6}\nabla^2\rho(\mathbf{r}) \qquad (3)$$

while the corresponding potential energy densities $V(\mathbf{r})$ at the bcp's were obtained from the local virial theorem

$$V(\mathbf{r}) = \frac{1}{4}\nabla^2\rho(\mathbf{r}) - 2G(\mathbf{r}) \qquad (4)$$

This approximation for $G(\mathbf{r})$ holds well in regions where $\nabla^2\rho(\mathbf{r}) > 0$[57] and is a good approximation for the transition-metal−ligand bonds. It is much less useful for bonds involving shared interactions, such as C−C and C−H bonds.

Integrated source functions were obtained from the basin integration routines in the XDPROP module of XD-2006,[45] using

(51) Su, Z.; Coppens, P. *Acta Crystallogr., Sect. A* **1998**, *54*, 646.
(52) Bunge, C. F.; Barrientos, J. A.; Bunge, A. V. *At. Data Nucl. Data Tables* **1993**, *53*, 113.
(53) Coppens, P. *Coord. Chem. Rev.* **1985**, *65*, 285.
(54) (a) Becker, P. J.; Coppens, P. *Acta Crystallogr., Sect. A* **1974**, *30*, 129. (b) Becker, P. J.; Coppens, P. *Acta Crystallogr., Sect. A* **1974**, *30*, 148. (c) Becker, P. J.; Coppens, P. *Acta Crystallogr., Sect. A* **1975**, *31*, 417.
(55) Hirshfeld, F. L. *Acta Crystallogr., Sect. A* **1976**, *32*, 239.
(56) Abramov, Y. A. *Acta Crystallogr., Sect. A* **1997**, *53*, 264.
(57) Gálvez, O.; Gómez, P. C.; Pacios, L. F. *Chem. Phys. Lett.* **2001**, *337*, 263.

Table 3. Bond Critical Point Properties for Complex **3**[a]

bond	d_1[b]	d_2[b]	$\rho(\mathbf{r}_{bcp})$[c]	$\nabla^2\rho(\mathbf{r}_{bcp})$[d]	λ_1[d]	λ_2[d]	λ_3[d]	ε	$G(\mathbf{r}_{bcp})$[e]	$G(\mathbf{r}_{bcp})/\rho(\mathbf{r}_{bcp})$	$V(\mathbf{r}_{bcp})$[e]	$\lvert V(\mathbf{r}_{bcp})\rvert/ G(\mathbf{r}_{bcp})$	$H(\mathbf{r}_{bcp})$[e]
Cr1−C2	1.132	1.184	0.41	4.88	−1.22	−0.07	6.16	17.4	0.41	1.00	−0.47	1.15	−0.06
	1.1168	*1.2299*	*0.39*	*4.87*	*−1.15*	*−0.05*	*6.06*	*23.2*	*0.40*	*1.01*	*−0.45*	*1.13*	*−0.06*
Cr1−C3	1.1152	1.2186	0.41	5.09	−1.16	−0.13	6.38	8.04	0.42	1.02	−0.48	1.14	−0.06
	1.1170	*1.2405*	*0.39*	*4.87*	*−1.15*	*−0.04*	*6.06*	*24.70*	*0.40*	*1.01*	*−0.45*	*1.13*	*−0.06*
Cr1−C4	0.9103	0.9345	0.88	13.19	−3.85	−3.28	20.33	0.17	1.26	1.44	−1.61	1.28	−0.34
	0.9306	*0.9356*	*0.84*	*11.78*	*−3.02*	*−2.85*	*17.65*	*0.06*	*1.12*	*1.33*	*−1.42*	*1.27*	*−0.30*
Cr1−C5	0.9122	0.9314	0.87	13.48	−3.78	−3.15	20.41	0.20	1.27	1.46	−1.50	1.18	−0.32
	0.9306	*0.9356*	*0.84*	*11.78*	*−3.02*	*−2.85*	*17.65*	*0.06*	*1.12*	*1.33*	*−1.42*	*1.27*	*−0.30*
C1−C1′	0.7021	0.7021	2.06	−17.38	−15.54	−12.22	10.38	0.27	1.87	0.91	−4.96	2.65	−3.09
	0.7000	*0.7000*	*2.06*	*−20.12*	*−15.97*	*−13.24*	*9.09*	*0.21*	*0.67*	*0.33*	*−2.76*	*4.12*	*−2.08*
C1−C2	0.6988	0.7204	2.00	−16.54	−14.75	−12.17	10.38	0.21	1.78	0.89	−4.72	2.65	−2.94
	0.7094	*0.7094*	*1.99*	*−18.79*	*−15.17*	*−12.98*	*9.36*	*0.17*	*0.61*	*0.31*	*−2.54*	*4.16*	*−1.93*
C2−C3	0.6990	0.7060	2.08	−17.67	−15.49	−12.55	10.37	0.23	1.90	0.91	−5.04	2.65	−3.14
	0.7000	*0.7000*	*2.06*	*−20.12*	*−15.97*	*−13.24*	*9.09*	*0.21*	*0.67*	*0.33*	*−2.76*	*4.12*	*−2.08*
C3−C3′	0.7114	0.7114	2.02	−16.49	−15.01	−12.11	10.63	0.24	1.82	0.90	−4.80	2.64	−2.98
	0.7094	*0.7094*	*1.99*	*−18.79*	*−15.17*	*−12.98*	*9.36*	*0.17*	*0.61*	*0.31*	*−2.54*	*4.16*	*−1.93*
C−O (ave)	0.40	0.75	3.25	−23	−33	−32	43	0.02	4.7	1.4	−11	2.3	−6.2
	0.39	*0.76*	*3.20*	*0.76*	*−34.4*	*−34.4*	*69.6*	*0.00*	*6.0*	*1.89*	*−12.0*	*2.0*	*−5.98*
C−H (ave)	0.37	0.71	1.91	−21	−18	−18	15	0.04	1.4	0.73	−4.2	3.0	−2.9
	0.39	*0.69*	*1.98*	*−26.91*	*−20.02*	*−19.75*	*12.85*	*0.01*	*0.25*	*0.13*	*−2.39*	*9.56*	*−2.14*

[a] For each compound, values in the first line are from experiment and those in the second line from the gas-phase DFT wave function. [b] d_1 and d_2 are the distances (Å) of the bcp to the nuclei. [c] Units of e Å^{-3}. [d] Units of e Å^{-5}. [e] Units of hartree Å^{-3}.

Table 4. Bond Critical Point Properties for Complex **4**[a]

bond	d_1[b]	d_2[b]	$\rho(\mathbf{r}_{bcp})$[c]	$\nabla^2\rho(\mathbf{r}_{bcp})$[d]	λ_1[d]	λ_2[d]	λ_3[d]	ε	$G(\mathbf{r}_{bcp})$[e]	$G(\mathbf{r}_{bcp})/\rho(\mathbf{r}_{bcp})$	$V(\mathbf{r}_{bcp})$[e]	$\lvert V(\mathbf{r}_{bcp})\rvert/ G(\mathbf{r}_{bcp})$	$H(\mathbf{r}_{bcp})$[e]
C_{C1-C4}−Fe1[f]	1.018	1.046	0.54	7.5	−1.8	−0.2	9.5	8	0.64	1.18	−0.75	1.2	−0.11
	1.031	*1.050*	*0.55*	*6.9*	*−1.7*	*−0.5*	*9.1*	*2.2*	*0.61*	*1.10*	*−0.73*	*1.2*	*−0.12*
C6−Fe1	1.028	1.0287	0.59	7.70	−2.01	−0.56	10.17	2.6	0.69	1.17	−0.85	1.23	−0.16
	1.0301	*1.0488*	*0.55*	*6.87*	*−1.70*	*−0.63*	*9.20*	*1.72*	*0.60*	*1.09*	*−0.73*	*1.22*	*−0.12*
C7−Fe1	1.0248	1.0349	0.59	7.50	−2.04	−0.46	10.0	3.42	0.68	1.16	−0.84	1.23	−0.16
	1.0312	*1.0515*	*0.55*	*6.98*	*−1.68*	*−0.48*	*9.15*	*2.49*	*0.61*	*1.11*	*−0.73*	*1.20*	*−0.12*
C8−Fe1	1.0267	1.0324	0.58	7.67	−1.95	−0.36	9.98	4.46	0.68	1.18	−0.83	1.22	−0.15
	1.0308	*1.0512*	*0.55*	*6.99*	*−1.68*	*−0.49*	*9.16*	*2.45*	*0.61*	*1.10*	*−0.73*	*1.20*	*−0.12*
C9−Fe1	1.0248	1.0294	0.59	7.85	−2.09	−0.55	10.49	2.77	0.70	1.19	−0.85	1.21	−0.15
	1.0295	*1.0492*	*0.56*	*6.85*	*−1.70*	*−0.64*	*9.19*	*1.66*	*0.60*	*1.09*	*−0.73*	*1.22*	*−0.12*
C10−Fe1[g]													
	1.0295	*1.0492*	*0.56*	*6.85*	*−1.70*	*−0.64*	*9.19*	*1.66*	*0.60*	*1.09*	*−0.73*	*1.22*	*−0.12*
C10−C11	0.7168	0.7339	1.96	−16.11	−14.84	−12.49	11.22	0.19	1.71	0.87	−4.54	2.65	−2.83
	0.6976	*0.7528*	*1.89*	*−17.72*	*−13.98*	*−12.08*	*8.34*	*0.16*	*0.49*	*0.26*	*−2.22*	*4.53*	*−1.73*
C11−C11′	0.6725	0.6725	2.42	−24.65	−20.76	−14.60	10.71	0.42	2.36	0.98	−6.45	2.73	−4.09
	0.6721	*0.6721*	*2.30*	*−24.29*	*−9.20*	*−12.24*	*7.16*	*0.57*	*0.88*	*0.38*	*−3.47*	*3.94*	*−2.58*
C11−F1	0.5434	0.8153	1.91	−9.71	−15.13	−13.74	19.16	0.10	1.92	1.00	−4.51	2.35	−2.6
	0.4582	*0.9092*	*1.63*	*3.04*	*−9.96*	*−9.63*	*22.63*	*0.03*	*2.31*	*1.42*	*−4.41*	*1.91*	*−2.10*
C−C[f]	0.713	0.717	2.13	−17.5	−16.6	−13.2	12.3	0.25	2.03	0.95	−5.3	2.61	−3.25
	0.713	*0.713*	*1.94*	*−17.3*	*−14.0*	*−11.3*	*8.0*	*0.24*	*0.65*	*0.34*	*−2.5*	*3.85*	*−1.86*
C−H[f]	0.387	0.689	2.03	−23.6	−20.2	−18.7	15.2	0.08	1.52	0.75	−4.70	3.09	−3.18
	0.385	*0.694*	*1.91*	*−23.5*	*−18.3*	*−17.9*	*12.7*	*0.02*	*0.25*	*0.13*	*−2.15*	*8.6*	*−1.90*
H9−F1′	1.1032	1.3876	0.05	1.13	−0.20	−0.14	1.47	0.41	0.06	1.17	−0.04	0.66	0.02
	1.0708	*1.3686*	*0.08*	*1.12*	*−0.26*	*−0.18*	*1.56*	*0.48*	*0.07*	*0.90*	*−0.06*	*0.85*	*0.01*

[a] For each compound, values in the first line are from experiment and those in the second line from the gas-phase DFT wave function. [b] d_1 and d_2 are the distances (Å) of the bcp to the nuclei. [c] Units of e Å^{-3}. [d] Units of e Å^{-5}. [e] Units of hartree Å^{-3}. [f] Averaged values. [g] No bcp was observed in the experimental topology.

a Lebedev−Laikov quadrature of 302 angular points. Plots of the scale factors[58] after the final multipole refinements (Figures S1 and S2 in the Supporting Information) showed no significant systematic deviations from linearity. The final residual Fourier maps for all three complexes were flat and essentially featureless (Figures S4, S7, and S11 in the Supporting Information), and the fractal dimension plots of the residual density[59] (Figure S3 in the Supporting Information) showed the idealized bell curves that are indicative of only random noise in the residuals. This demonstrates that no unmodeled information remained in the data. A small shoulder at positive density for compound **4** was attributed to the residuals associated with the excess thermal motion of the free Cp ring.

Theoretical Studies. DFT/B3LYP wave functions with full geometry optimization were obtained for **2**−**4** using the Pople 6-311++G(2d,2p) bases[60] for the light atoms and Wachters+f bases[61] for the transition metals. These were used to provide a reference density for comparison with the experimental results. In

(58) Zhurov, V. I.; Zhurova, E. A.; Pinkerton, A. A. *J. Appl. Crystallogr.* **2008**, *41*, 340.
(59) Meindl, K.; Henn, J. *Acta Crystallogr., Sect. A* **2008**, *64*, 404.
(60) (a) Krishnan, R.; Binkley, J. S.; Seeger, R.; Pople, J. A. *J. Chem. Phys.* **1980**, *72*, 650. (b) Frisch, M. J.; Pople, J. A.; Binkley, J. S. *J. Chem. Phys.* **1984**, *80*, 3265.
(61) (a) Wachters, J. H. *J. Chem. Phys.* **1970**, *52*, 1033. (b) Bauschlicher, C. W., Jr.; Langhoff, S. R.; Barnes, L. A. *J. Chem. Phys.* **1989**, *91*, 2399.

view of the lower experimental symmetry of **3**, stuctures were optimized both with and without full C_{3v} symmetry constraints. For the homologous series of 18-electron model compounds **I**−**VI** having the formula (η^n-C_nH_n)M(CO)$_3$ with varying ring sizes n (**I**, n = 3, M = Co; **II**, n = 4, M = Fe; **III**, n = 5, M = Mn; **IV**, n = 6, M = Cr; **V**, n = 7, M = V; and **VI**, n = 8, M = Ti), the slightly less extensive 6-311G** basis for all of the light atoms was used for geometry optimization. The molecular symmetry was held at C_s for all of the compounds except **I** and **IV**, where C_{3v} symmetry was imposed. For purposes of comparison with the other model compounds, calculations on **2** and **3** (i.e., models **III** and **IV**) were also carried out at this level. Frequency calculations established all of the optimized structures as local minima. In line with Hoffmann and co-workers[21] and Low and Hall[62] and at variance with Gadre and co-workers,[63] we found that the experimental staggered structure is the ground state structure for **3**. All of the computations were undertaken with the GAMESS-UK[64] or GAUSSIAN03[65] codes using basis sets obtained from EMSL.[66] The topologies and integrated properties of the Kohn−Sham densities were analyzed using the AIMPAC,[67] AIM2000,[68] or MORPHY[69] programs. Delocalization indices $\delta(\Omega_A, \Omega_B)$ were computed from the DFT wave functions using the approximation for the second-order density matrix, which generally gives values close to those obtained from HF wave functions.[70] The integrated source function was obtained from the DFT wave functions using a special version of the PROAIMV code,[67] kindly supplied by Dr. Carlo Gatti. Complex static X-ray structure factors to a resolution of (sin θ)/$\lambda \leq 1.1$ Å^{-1} were obtained from the molecular wave function by numerical integration of the charge density for reciprocal lattice points corresponding to a pseudocubic unit cell with a = 30 Å using the program WFN2HKL.[71] Periodic DFT/B3LYP calculations using the CRYSTAL06[72] code were also undertaken for complexes **2** and **3**, using the experimentally determined atomic coordinates and a standard 6-31G basis. As in the molecular calculations, static X-ray structure factors to a resolution of (sin θ)/$\lambda \leq 1.1$ Å^{-1} were computed from the periodic wave function. Multipole refinements against both of these synthetic data sets using XDLSM were undertaken to validate the transition-metal model used for the experimental data.

Results and Discussion

Description of the Structures. The crystal structures of (η^5-C_5H_5)Mn(CO)$_3$ (**2**)[73] and (η^6-C_6H_6)Cr(CO)$_3$ (**3**)[27a,74] are well-established. The preparation and crystal structure of (*E*)-{(η^5-C_5H_4)CF=CF(η^5-C_5H_4)}(η^5-C_5H_5)$_2$Fe$_2$ (**4**) has recently been reported.[34] ORTEP diagrams taken from the multipole refinements are shown in Figure 1. Molecules of **2** sit in general positions in the unit cell, while molecules of **3** and **4** reside on crystallographic symmetry elements (mirror plane and inversion

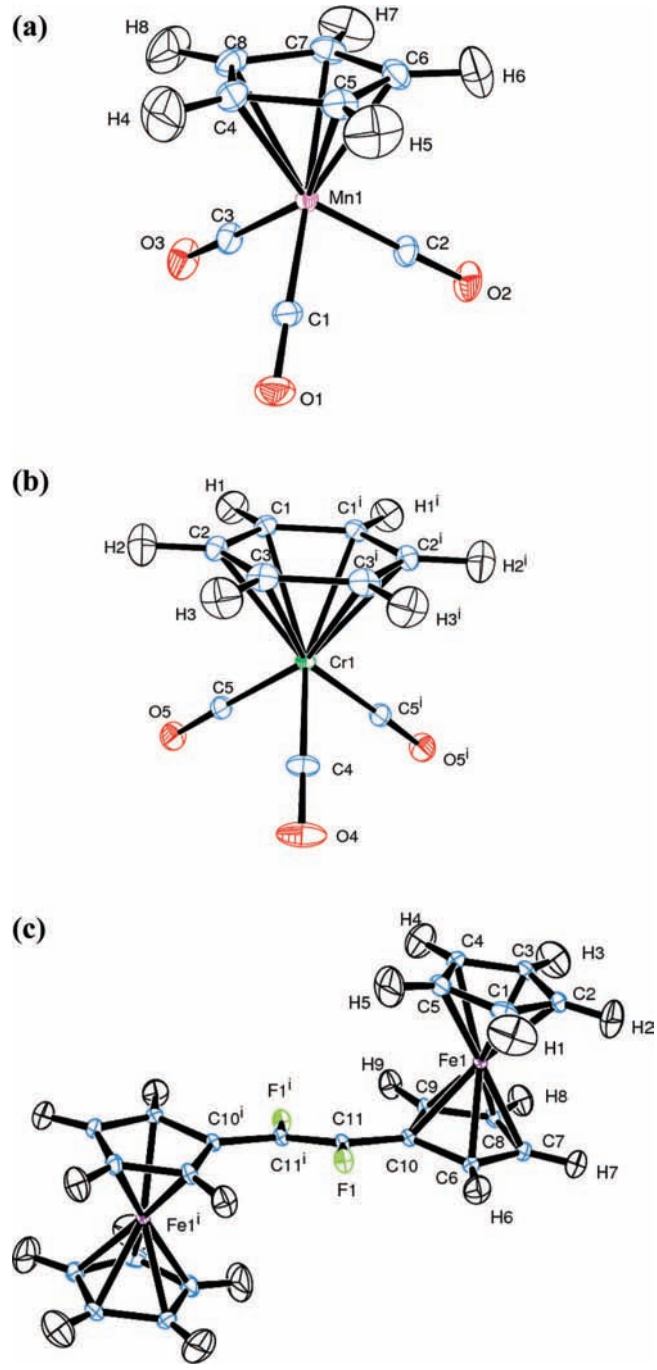

Figure 1. ORTEP diagrams showing the atomic labeling schemes for (a) (η^5-C_5H_5)Mn(CO)$_3$ (**2**), (η^6-C_6H_6)Cr(CO)$_3$ (**3**), and (*E*)-{(η^5-C_5H_4)CF=CF(η^5-C_5H_4)}(η^5-C_5H_5)$_2$Fe$_2$ (**4**). Thermal ellipsoids are drawn at the 50% probability level.

(62) Low, A. A.; Hall, M. B. *Int. J. Quantum Chem.* **2000**, *77*, 152.
(63) Suresh, C. H.; Koga, N.; Gadre, S. R. *Organometallics* **2000**, *19*, 3008.
(64) Guest, M. F.; Bush, I. J.; van Dam, H. J. J.; Sherwood, P.; Thomas, J. M. H.; van Lenthe, J. H.; Havenith, R. W. A.; Kendrick, J. *Mol. Phys.* **2005**, *103*, 719.
(65) Frisch, M. J.; et al. *Gaussian 03*, revision D.02; Gaussian, Inc.: Wallingford, CT, 2004.
(66) (a) Feller, D. *J. Comput. Chem.* **1996**, *17*, 1571. (b) Schuchardt, K. L.; Didier, B. T.; Elsethagen, T.; Sun, L.; Gurumoorthi, V.; Chase, J.; Li, J.; Windus, T. L. *J. Chem. Inf. Model.* **2007**, *47*, 1045.
(67) Biegler-König, F. W.; Bader, R. F. W.; Tang, T.-H. *J. Comput. Chem.* **1982**, *3*, 317.
(68) Biegler-König, F. *J. Comput. Chem.* **2000**, *12*, 1040.
(69) Popelier, P. L. A. *MORPHY98*; University of Manchester: Manchester, U.K., 1998.
(70) (a) Poater, J.; Solà, M.; Duran, M.; Fradera, X. *Theor. Chim. Acta* **2002**, *107*, 362. (b) Kar, T.; Ángyán, J. G.; Sannigrahi, A. B. *J. Phys. Chem. A* **2000**, *104*, 9953.
(71) Volkov, A. V. *WFN2HKL: A Parallellized Program for Calculation of Static Structure Factors from Electron Densities Represented with Gaussian- And Slater-Type Functions*; Middle Tennessee State University: Murfreesboro, TN, 2008.
(72) Dovesi, R.; Saunders, V. R.; Roetti, C.; Orlando, R.; Zicovich-Wilson, C. M.; Pascale, F.; Civalleri, B.; Doll, K.; Harrison, N. M.; Bush, I. J.; D'Arco, P.; Llunell, M. *CRYSTAL06 User's Manual*; University of Torino: Torino, Italy, 2006.
(73) (a) Berndt, A. F.; Marsh, R. E. *Acta Crystallogr.* **1963**, *16*, 118. (b) Fitzpatrick, P. J.; Le Page, Y.; Sedman, J.; Butler, I. S. *Inorg. Chem.* **1981**, *20*, 2852. (c) Cowie, J.; Hamilton, E. J. M.; Laurie, J. C. V.; Welch, A. J. *J. Organomet. Chem.* **1990**, *394*, 1. (d) Kawano, M.; Kobayashi, Y.; Ozeki, T.; Fujita, M. *J. Am. Chem. Soc.* **2006**, *128*, 6558.

center, respectively). A complete listing of bond distances and bond angles is provided in the Supporting Information in CIF format.

The structural parameters for **2** and **3** are the most precise ones determined for these molecules to date. Complex **2** has C_1 symmetry, with the Mn−C(Cp) distances in the range 2.1461(3)−2.1510(3) Å. This very small range of only 16σ indicates an insignificant ring-slippage distortion. The C−C distances vary more, with a range of 0.0166 Å (i.e., 33σ); the longest C−C distance occurs for the C4−C5 bond, which is most fully eclipsed by a carbonyl ligand (C1−O1, see Figure S16 in the Supporting Information). As was established in a previous structural determination,[27a] complex **3** has close to idealized C_{3v} symmetry and adopts the staggered conformation, where the C−O bond vectors eclipse alternate C−C bonds. It shows a partial localization of double-bond character around the ring, as the three bonds eclipsed by the CO ligands average 1.4208(4) Å and are ∼0.016 Å longer than the noneclipsed bonds, which average 1.4044(4) Å. This difference is identical to that reported in a microwave study of **3** in the gas phase[75] and is also well-reproduced in our DFT/B3LYP optimized structure, where Δ(C−C) is 0.019 Å. However, the experimental structure shows a greater range of $Cr-C_{benzene}$ distances [2.22160(16)−2.24189(14) Å] than the optimized structure (2.248−2.249 Å).

Complex **4** exhibits almost perfectly eclipsed C_5 rings, with a mean $C-cent_A-cent_B-C$ torsion angle of 0.3° ($cent_A$ and $cent_B$ are the unweighted centroids of the two C_5 rings). This gives rise to local D_{5h} symmetry, as found in the ground-state structure of the parent, ferrocene.[4] The Fe−C distances fall in a narrow range and are essentially identical for the two rings, with $Fe-C_{C1-C5} = 2.053 \pm 0.006$ Å and $Fe-C_{C6-C10} = 2.050 \pm 0.004$ Å. This is indicative of near-idealized η^5 geometries for both rings. As expected, the free Cp ring C1−C5 displays a greater in-plane thermal motion than the substituted ring C6−C10. The mean Δ(msda) values for the $Fe-C_{ring}$ bonds are 2.0×10^{-3} and 1.5×10^{-3} Å^2 for the free and substituted rings, respectively. A TLS analysis[76] shows that the libration tensor **L** for the C1−C5 thermal motion is highly anisotropic, with the principal direction almost parallel to the $Fe-C_5$ fivefold axis. On the other hand, the librational motion of the C6−C10 ring is less pronounced and more isotropic. The principal axis is approximately parallel to the C10−C11 bond vector. Further details are given in Tables S1 and S2 and Figure S34 in the Supporting Information. The effects of thermal motion may be seen in the residual maps for **4**, where the strongest features are found near the C1−C5 ring. The other feature of interest in the crystal structure of **4** is the relatively short C−F···F−C intermolecular contact of 2.7007(5) Å parallel to the crystallographic *c* axis (see Figure S15 in the Supporting Information). Short halogen−halogen interactions in crystal packings have been noted for some time, and their nature is a subject of some interest.[77]

Topological Properties and Molecular Graphs. Two previous charge density studies[27a,74c] on **3** were undertaken in an era before QTAIM topological analysis was widely utilized. The dynamic deformation density maps obtained for **3** are given in the Supporting Information and are reasonably similar to those from these previous studies,[27a,74c] though the significantly lower residuals in our study indicate that the CCD data are more accurate. The experimental and theoretical bcp properties for compounds **2**−**4** are given in Tables 2−4, respectively. The agreement between experiment and theory is excellent in general, and the only noticeable discrepancy concerns the C−F bond in **4**. For this interaction, the experimental $\rho(\mathbf{r}_{bcp})$ is significantly greater and the experimental $\nabla^2\rho(\mathbf{r}_{bcp})$ more negative than the theoretical values. This effect been noted previously[78] and can be ascribed mainly to the differing locations of the C−F bcp.

When chemical interactions in transition-metal compounds are being characterized in terms of the chemical topology, it is important to bear in mind that a broader spectrum of topological indicators than just the "orthodox" ones [i.e., the magnitudes of $\rho(\mathbf{r}_{bcp})$ and $\nabla^2\rho(\mathbf{r}_{bcp})$] needs to be considered. The reader is directed to recent reviews[79] that discuss this topic comprehensively. We note here that the magnitudes of $\rho(\mathbf{r}_{bcp})$ and $\nabla^2\rho(\mathbf{r}_{bcp})$ for the M−C bonding interactions in Tables 2−4 are quite typical for organo−transition-metal complexes[15,79] and within context may be taken to indicate significant covalency. The total energy density H is negative for all of the M−C bonding interactions, which may also be taken as an indicator of covalency.[80] In terms of the metal−ring interaction, the significantly less negative values of H for the $M-C_{ring}$ interactions than for the $M-C_{CO}$ interactions may be taken as a signal of a weaker covalent interaction.

The experimental molecular graphs of **2**−**4**, shown in Figure 2, immediately illustrate the difficulties of using a localized bond path approach to understand the metal−ring bonding. The theoretical molecular graph of **2** shows the [5, 5, 1 + 1] topology, but the experimental graph shows only four Mn−C bond paths. Interestingly the missing bond path for Mn1−C7 is associated with the *shortest* rather than the longest $Mn-C_{Cp}$ distance. Moreover, the ring and bond cp's for one of these bond paths, Mn1−C5, are extremely close together (0.02 Å). With the nearly zero value for λ_2, this gives rise to a very high ellipticity and a bond path close to an annihilation event. Indeed, with some multipole refinement models, this bond path was not observed at all. Likewise, in complex **4**, while the theoretical graph shows the [5, 5, 0 + 0] topology, in the experimental graph there are only four bond paths between the Fe center and each of the two chemically distinct Cp rings, with the C_5 ccp and associated rcp missing in both cases. The missing bond paths are associated with C5 and C10, the substituted C_{ring} atom and the C atom that eclipses this atom, i.e., with the *longest* (or *near longest*) $Fe-C_{ring}$ distances. This contrasts with the situation observed for **2** and clearly shows that the absence of the $M-C_{ring}$ bond paths is not an issue related simply to the $M-C_{ring}$ distances.[81]

The situation for complex **3** is more intriguing. Both the experimental and theoretical molecular graphs show only three bond paths between the Cr atom and the benzene ring, instead

(74) (a) Bailey, M. F.; Dahl, L. F. *Inorg. Chem.* **1965**, *4*, 1314. (b) Allegra, G.; Natta, G. *Atti Accad. Naz. Lincei* **1961**, *31*, 241. (c) Wang, Y.; Angermund, K.; Goddard, R.; Kruger, C. *J. Am. Chem. Soc.* **1987**, *109*, 587.
(75) Kukoloch, S. G. *J. Am. Chem. Soc.* **1995**, *117*, 5512.
(76) Schomaker, V.; Trueblood, K. N. *Acta Crystallogr., Sect. B* **1968**, *24*, 63.
(77) Desiraju, G. R.; Parthasarathy, R. *J. Am. Chem. Soc.* **1989**, *111*, 8725.
(78) (a) Lentz, D.; Bach, A.; Buschmann, J.; Luger, P.; Messerschmidt, M. *Chem.—Eur. J.* **2004**, *10*, 5059. (b) Bach, A.; Lentz, D.; Luger, P. *J. Phys. Chem. A* **2001**, *105*, 7405.
(79) (a) Macchi, P.; Sironi, A. *Coord. Chem. Rev.* **2003**, *238*, 383, and references therein. (b) Gatti, C. *Z. Kristallogr.* **2005**, *220*, 399, and references therein.
(80) Cremer, D.; Kraka, E. *Croat. Chem. Acta* **1984**, *57*, 1259.

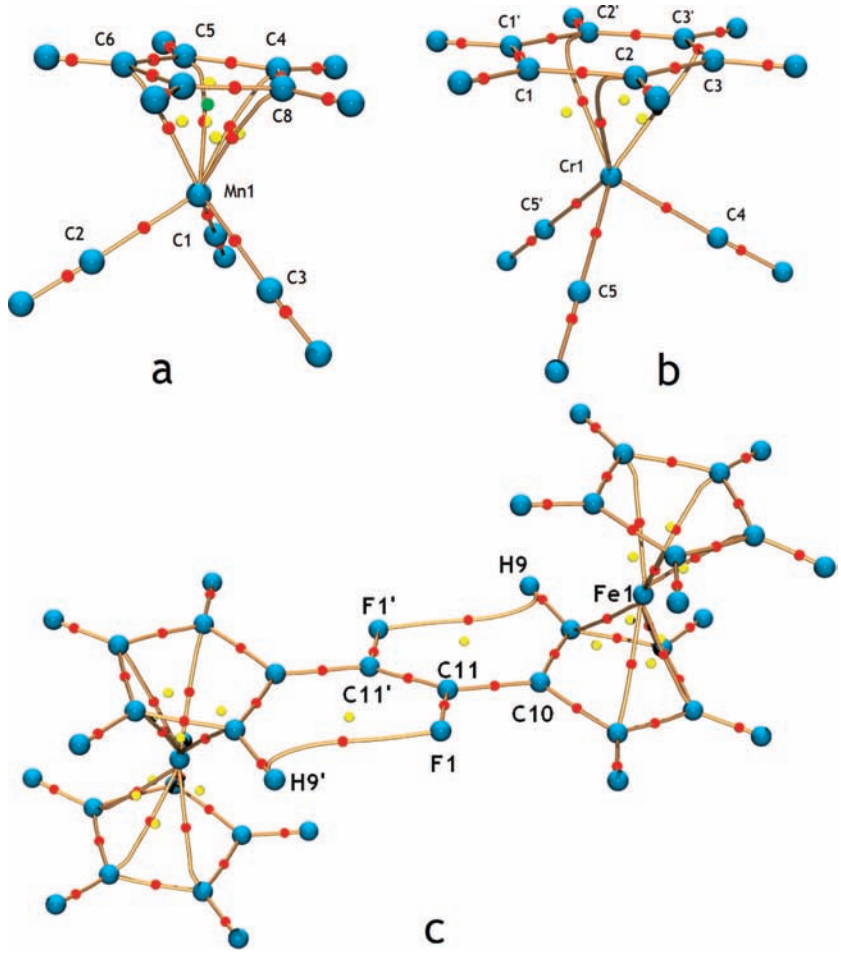

Figure 2. Experimental molecular graphs of (a) (η^5-C_5H_5)$Mn(CO)_3$ (**2**), (b) (η^6-C_6H_6)$Cr(CO)_3$ (**3**) and (c) (*E*)-{(η^5-C_5H_4)CF═CF(η^5-C_5H_4)}(η^5-C_5H_5)$_2Fe_2$ (**4**). Bond critical points are shown in red, ring critical points in yellow, and cage critical points in green.

of the expected six. Moreover, both graphs show an unusual "T-shaped" bond path from the Cr center that has as its other attractor not a C atom of the benzene ring but the bcp associated with a ring C−C bond. This feature represents an unstable conflict structure associated with a bifurcation catastophe,[11] and it is striking that it is observed in both the experimental and theoretical graphs. If molecular C_{3v} symmetry is imposed in the DFT geometry optimization, then all three Cr−$C_{benzene}$ bond paths in the resulting graph are of this kind (though we have never observed this situation in any experimental graph). The "T-shaped" bond path has previously been associated with a dominating electrostatic component of the bonding in alkene and alkyne complexes,[82] but this conclusion does not seem appropriate for complex **3**. Moreover, since this feature is an unstable topological object, we expect that any small perturbation would lead to termination of the bond path on one or the other of the C atoms, as found for the other Cr−C_{ring} bond paths in **3**. Combined with the three bond paths to the carbonyl ligands, the coordination geometry at the Cr center is trigonal prismatic. Interestingly, Gadre and co-workers[63] also reported only three M−C_{ring} bond paths in the eclipsed conformation of **3**, which terminate on the eclipsed ring-C atom. They also found only three M−C_{ring} interaction lines in the topology of the electrostatic field $\phi(\mathbf{r})$. As was observed for **2** and **4**, the Cr−$C_{benzene}$ bond paths are associated with very high ellipticities, which is a consequence of the fact that these critical points occur in a region of very flat density and cannot be taken as any indicator of M−C_{ring} π bonding. The C_6 rcp and ccp are also missing from both the experimental and theoretical topologies. We are aware of only one other report on the experimental topology in a metal−benzene complex, by Lyssenko et al.[83] They observed all six Cr−C bond paths for each Cr(η^6-C_6H_6) interaction in Cr(η^6-C_6H_6)$_2$, though again the C_6 rcp and ccp were missing.

To further explore the topology of carbocyclic systems, we examined the theoretical molecular graphs of the homologous

(81) Interestingly, in a recent independent study of 1,1′-disubstituted ferrocenes, bond paths were lacking in the case of the shortest Fe−C distances. See: Makal, A.; Plażuk, D.; Zakrzewski, J.; Misterkiewicz, R.; Wożniak, K. *Fifth European Charge Density Meeting*, Gravedona, Italy, June 6−11, 2008; poster P55.

(82) A similar "T-shaped" bond path was reported by Frenking and co-workers for the electrostatic Cu−alkene interaction in $[Cu(C_2H_4)]^+$ (see: Böhme, M.; Wagener, T.; Frenking, G. *J. Organomet. Chem.* **1996**, *520*, 31). In line with the expected instability of this structure, we note that Hertwig et al. found a ring structure for the same interaction (see: Hertwig, R. H.; Koch, W.; Schröder, D.; Schwartz, H.; Hrušák, J.; Schwerdtfeger, P. *J. Phys. Chem.* **1996**, *100*, 12253.) More recently, Scherer and co-workers have reported similar "T-shaped" bond paths in the experimental molecular graphs of Ag−acetylene complexes (see refs 25b–d) and scandium carbide complexes (see: Rohrmoser, B.; Eickerling, G.; Presnitz, M.; Scherer, W.; Eyert, V.; Hoffmann, R.-D.; Rodewald, U. C.; Vogt, C.; Pöttgen, R. *J. Am. Chem. Soc.* **2007**, *129*, 9356.)

(83) Lyssenko, K. A.; Korlyukov, A. A.; Golovanov, D. G.; Ketkov, S. Yu.; Antipin, M. Yu. *J. Phys. Chem. A* **2006**, *110*, 6545.

series **I**−**VI** of 18-electron complexes (η^n-C_nH_n)$M(CO)_3$ with varying ring sizes n. These complexes (or closely related derivatives) are known compounds,[84−87] apart from the hypothetical **VI**. To examine any basis-set dependencies, two basis sets were used: standard Pople 6-311G** basis sets[60] for the light atoms and the Wachters+f basis set for the metals[61] (BASIS A) and the Alhrichs VTZ[88] basis for all centers (BASIS B). In addition to the molecular graphs, we also present in Figure 3 the corresponding graphs of $V(\mathbf{r})$, the potential energy density (or virial field). The graphs in Figure 3 reveal several interesting points. First, the molecular and virial graphs are not in general homeomorphic because the systems lie close to catastrophe points.[89] The virial graphs show less basis-set dependency and exhibit interaction lines between the metal atom and all of the C_{ring} atoms, which are indicative of energy lowering and hence chemical bonding in the QTAIM sense[12] between all these centers. Second, the molecular graphs for $n > 5$ show an obvious basis-set dependence, which we again ascribe to fact that the structures lie close to catastrophe points. Finally, the C_n rcp and its associated ccp are not present in either the molecular or virial graph for $n > 5$, though this may be as much related to the changing metal atom as to the ring size. We conclude that in the ideal case, the M(η^n-C_nH_n) system should give rise to a ring of n bcp's interspersed with n rcp's, the $[n, n]$ topology. However, this constellation of cp's is an unstable topological object, and deviations from the idealized geometry may lead to unpredictable catastrophe situations and the coalescence of pairs of bcp's and rcp's. This instability increases with increasing n because the bcp's and rcp's are necessarily closer in space, and in real complexes, this idealized M−ring topology may not be realized for $n \geq 5$. In the C_{2v} Jahn−Teller-distorted metallocenes Cr(η^5-C_5H_5)$_2$ and Co(η^5-C_5H_5)$_2$, for instance, only three M−C_{ring} bond paths were observed for each ring.[16]

In order to investigate cases where the distortion in the metal−η^n-hydrocarbyl interaction is sufficiently great to lead to a formal reduction in the hapticity, we examined the theoretical charge densities in two additional model complexes: Cr(η^5-C_5H_5)(η^3-C_5H_5)$(CO)_2$ (**VII**) and Fe(η^6-C_8H_8)(η^4-C_8H_8) (**VIII**).[90] The optimized geometries are shown in Figures 4 and 5, respectively. The formal η^5-C_5H_5 ring in **VII** shows a significant ene−allyl slippage, which is much more pronounced for the formal η^3-C_5H_5 ring. Bond paths are observed only for the four shortest Cr−C_{ring} distances in **VII**, which are less than 2.3 Å, giving rise to three bond paths to the formal η^5-ring and a single bond path to the formal η^3 ring. A similar situation pertains in **VIII**, where two bond paths to the formal η^6 ring are associated with the two shortest Fe−C distances and a single bond path to the formal η^4 ring is again associated with the

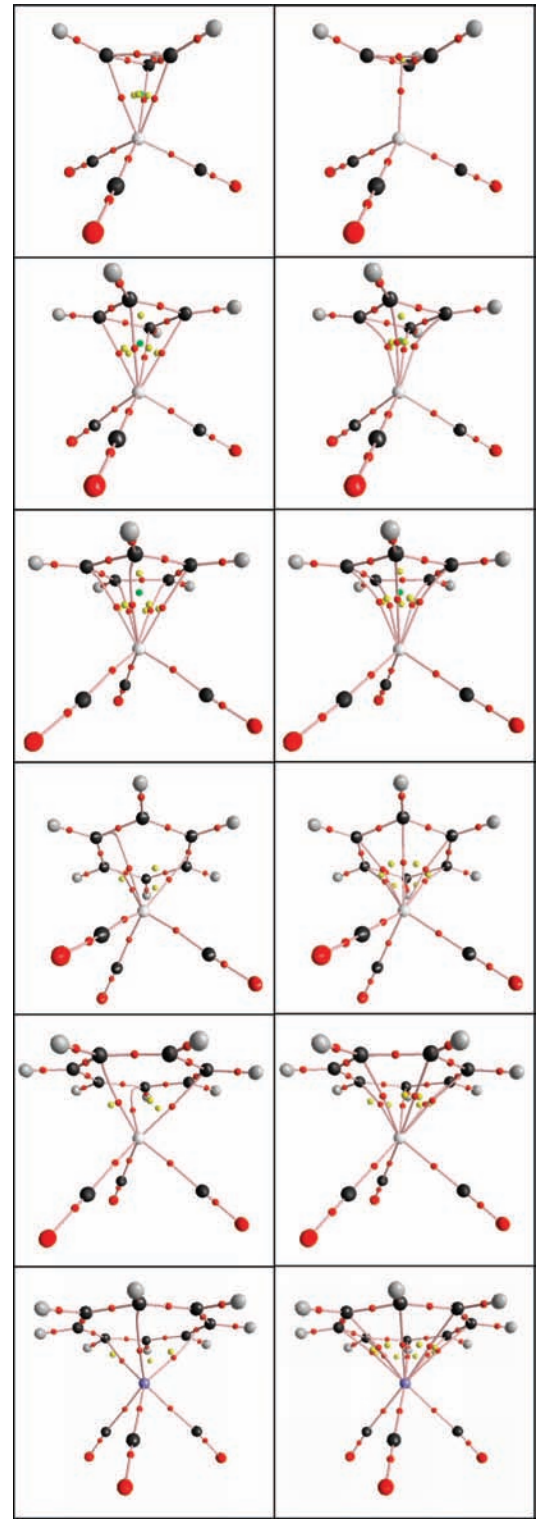

Figure 3. Theoretical graphs of the complexes (η^n-C_nH_n)$M(CO)_3$ (**I**−**VI**) in the scalar fields of (left) the electron density $\rho(\mathbf{r})$ (molecular graphs) and (right) the potential energy density $V(\mathbf{r})$ (virial graphs), obtained using BASIS A (see text). The critical points are color-coded: (3, +3) cp's in green, (3, +1) cp's in yellow, and (3, −1) cp's in red. In order from top to bottom: **I**, M = Co, $n = 3$; **II**, M = Fe, $n = 4$; **III**, M = Mn, $n = 5$; **IV**, M = Cr, $n = 6$; **V**, M = V, $n = 7$; **VI**, M = Ti, $n = 8$. The corresponding graphs for BASIS B are given in Figure S33 in the Supporting Information.

(84) The unsubstituted η^3-cyclopropenyl complex (η^3-C_3H_3)$Co(CO)_3$ is unknown, although derivatives such as (η^3-C_3Ph_3)$Co(CO)_3$ (see: Chiang, T.; Kerber, R. C.; Kimball, S. D.; Lauher, J. W. *Inorg. Chem.* **1979**, *18*, 1687) and (η^3-$C_3Bu^t_3$)$Co(CO)_3$ (see:Hughes, R. P.; Tucker, D. S.; Rheingold, A. L. *Organometallics* **1993**, *12*, 3069.) are well-characterized.

(85) The structure of (η^4-C_4H_4)$Fe(CO)_3$ has been determined. See: Harvey, P. D.; Schaefer, W. P.; Gray, H. B.; Gilson, D. F. R.; Butler, I. S. *Inorg. Chem.* **1988**, *27*, 57.

(86) The complex (η^7-C_7H_7)$V(CO)_3$ was first reported in 1961 (see: Werner, R. P. M.; Manastyrskyj, S. A. *J. Am. Chem. Soc.* **1961**, *83*, 2023), and its structure has been determined, though no atomic coordinates are available (see:Allegra, G.; Perego, G. *Ric. Sci., Parte 2, Sez. A* **1961**, *1*, 362.). However, (η^7-C_7H_7)(η^5-C_5H_5)V and numerous derivatives have been structurally characterized (see, for example, ref 27g)

(87) The 18-electron carbonyl complex (η^8-C_8H_8)$Ti(CO)_3$ is unknown, though related complexes such as (η^8-C_8H_8)(η^5-C_5H_5)Ti have been structurally characterized (see ref 27g).

(88) Schafer, A.; Horn, H.; Ahlrichs, R. *J. Chem. Phys.* **1992**, *97*, 2571.

(89) Keith, T. A.; Bader, R. F. W.; Aray, Y. *Int. J. Quantum Chem.* **1996**, *57*, 183.

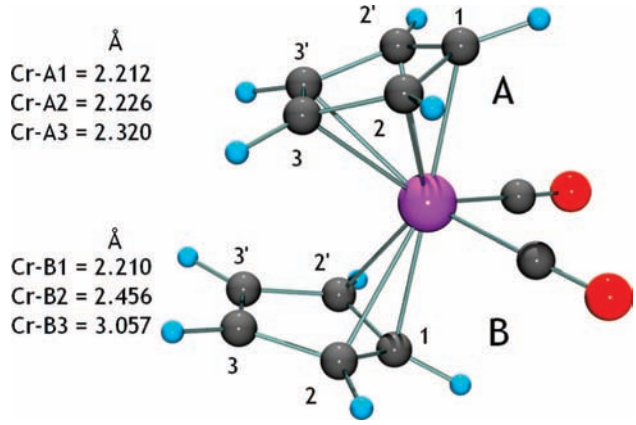

Figure 4. DFT-optimized structure of Cr(η^5-C_5H_5)(η^3-C_5H_5)$(CO)_2$ (**VII**).

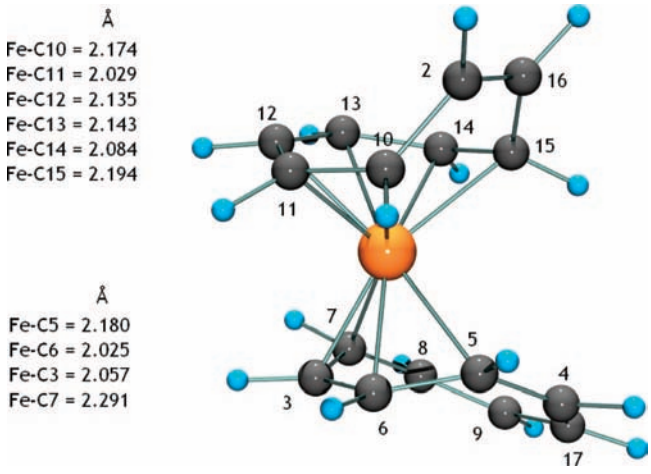

Figure 5. DFT-optimized structure of Fe(η^6-C_8H_8)(η^4-C_8H_8) (**VIII**).

shortest Fe−C distance. The molecular and virial graphs for **VII** and **VIII** are given in Figures S21 and S22, respectively, in the Supporting Information. It is clear that the formal hapticity does not provide much indication as to the number of bond paths observed in the molecular graph.

It is instructive to examine in more detail the features of the charge density, $\rho(\mathbf{r})$, and the gradient of the charge density, $\nabla\rho(\mathbf{r})$, in the plane of the ring of bcp's and rcp's. Plots of ρ and $\nabla\rho$ for the experimental pro-molecule density ρ_{pro} and molecular density ρ_{mol}[91] in compound **2** in this plane are shown in Figure 6. For both the ρ_{pro} and ρ_{mol} densities, only a narrow annulus of very low values of $\nabla\rho(\mathbf{r})$ is observed, delimiting the region in which any bcp's and rcp's must occur. For the ρ_{pro} density, five minima in $\nabla\rho(\mathbf{r})$, corresponding to the bcp's, are clearly visible in Figure 6c, and the set of five local maxima in the plot of $\rho(\mathbf{r})$ are also obvious. As a result, the five Mn−C_{ring} bcp's are well-defined, having identical density values [$\rho(\mathbf{r}) \approx 0.49$ e Å^{-3}], relatively large λ_2 values [$\lambda_2 \approx -0.43 \pm 0.02$ e Å^{-5}], and relatively low ellipticity values [$\varepsilon \approx 1.2-1.3$]. On the other hand, for the density ρ_{mol}, we have seen that one bcp is missing. While the values of $\rho(\mathbf{r})$ are very similar, the magnitudes of λ_2 are small, and the corresponding values of ε are larger and much more variable (see Table 2). Switching on the interaction between atoms of course leads to a considerable delocalization of density among the C atoms of the ring, which is obvious in Figure 6. This delocalization results an inner torus of very flat density in which the cp's are located and to an annulus of very low $\nabla\rho(\mathbf{r})$ where the minima are less well defined.

The corresponding plots of $\nabla\rho(\mathbf{r})$ in the planes of the critical point(s) for compounds **VII** and **VIII** are shown in Figure 7. In the case of **VII**, the formal η^5 ring generates an annulus of very low $\nabla\rho(\mathbf{r})$ analogous to that seen for **2**, but for the formal η^3 C_5H_5 ring, only a single small zone of very low $\nabla\rho(\mathbf{r})$ is seen. Taken together with the virial graph, which shows only a single Cr−C interaction line to this ring, this implies that the formal η^3 C_5H_5 ring may more correctly be treated as an η^1 C_5H_5 ring, suggesting a 16-electron rather than an 18-electron situation for **VII**. For complex **VIII**, there are open annuli corresponding to the formal η^4 and η^6 C_8H_8 rings. The reader cannot fail to notice the similarity between the annuli of low $\nabla\rho(\mathbf{r})$ values in Figures 6 and 7 and the graphical symbols commonly used in chemical-structure diagrams to represent the delocalized interactions between transition-metal atoms and open or closed conjugated π systems. These symbols are thus highly appropriate for representing the delocalized topological interaction[20] of the metal density with the ring density.

Discrepancies between the experimental and theoretical topologies of $\rho(\mathbf{r})$, as shown above for **2** and **4**, have been noted frequently. They could arise from several causes, including but not limited to errors in the experimental structure factors, basis-set limitations, the electron-correlation level, and multipole-model inadequacies. One potential cause which can definitely be discounted in our experimental studies is the well-known limitations[92] of the Hansen−Coppens multipole model. Multipole models for **2** and **4** obtained by refinements against static structure factors obtained from the DFT gas-phase wave function afford molecular graphs identical to those obtained by direct analysis of the quantum electron density from the same wave function.

In conclusion then, the observed number of bond paths between metal atoms and π-carbocyclic ligands is unlikely to reflect the formal hapticity. The virial graphs of complexes **I**−**VI** do indeed show that there is chemical bonding[12] between the metal and all of the C atoms in the ring, in compliance with chemical sense. While it is generally observed that the molecular and virial graphs are homeomorphic,[89] this may not always be the case when the equilibrium structure is close to a catastrophe point, which is of course the situation here. In view of this,

(90) Compound **VII** does not appear to have been isolated, though spectroscopic evidence for its existence has been presented. See: (a) van Raaij, E. U.; Brintzinger, H.-H. *J. Organomet. Chem.* **1988**, *356*, 315. (b) Millar, J. M.; Kastrup, R. V.; Harris, S.; Horváth, I. T. *Angew. Chem., Int. Ed. Engl.* **1990**, *29*, 194. A PRDDO optimized structure has also appeared. See: (c) Lawless, M. S.; Marynick, D. S. *Organometallics* **1991**, *10*, 543. A crystal structure of the W analog of **VII** has been reported. See: (d) Huttner, G.; Brintzinger, H. H.; Bell, L. G.; Friederich, P.; Bejenke, V.; Neugebauer, D. *J. Organomet. Chem.* **1978**, *145*, 329. The crystal structure of **VIII** has been reported but unfortunately is seriously affected by disorder. See: (e) Allegra, G.; Colombo, A.; Mognaschi, E. R. *Gazz. Chim. Ital.* **1972**, *102*, 1060.

(91) The pro-molecule density ρ_{pro} is the sum of the densities of noninteracting spherical atoms placed at the nuclear positions, while the molecular density ρ_{mol} is derived from the experimental multipole parameters.

(92) (a) Swaminathan, S.; Craven, B. M.; Spackman, M. A.; Stewart, R. F. *Acta Crystallogr., Sect. B* **1984**, *40*, 398. (b) Iversen, B. B.; Larsen, F. K.; Figgis, B. N.; Reynolds, P. A. *J. Chem. Soc., Dalton Trans.* **1997**, 2227. (c) Volkov, A.; Abramov, Y.; Coppens, P.; Gatti, C. *Acta Crystallogr., Sect. A* **2000**, *56*, 332. (d) Volkov, A.; Abramov, Y.; Coppens, P. *Acta Crystallogr., Sect. A* **2001**, *57*, 272. (e) Volkov, A.; Coppens, P. *Acta Crystallogr., Sect. A* **2001**, *57*, 395. (f) Koritsanszky, T.; Volkov, A. *Chem. Phys. Lett.* **2004**, *385*, 431.

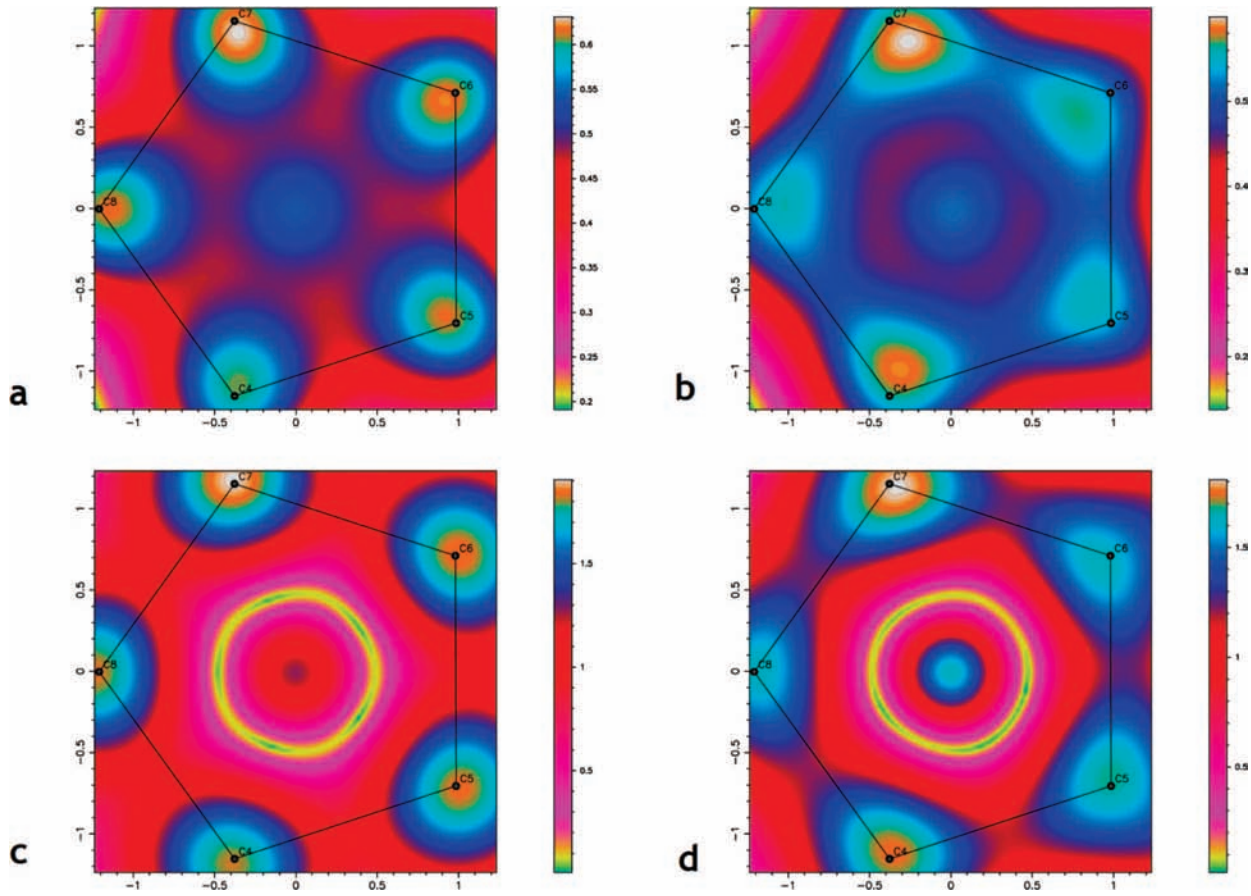

Figure 6. (a, b) Experimental charge density $\rho(\mathbf{r})$ and (c, d) its gradient $\nabla\rho(\mathbf{r})$ in the plane of the bcp's parallel to the C_5 ring in $(\eta^5\text{-}C_5H_5)Mn(CO)_3$ (**2**). Plots (a) and (c) refer to the pro-molecule density ρ_{pro} and plots (b) and (d) to the experimental molecular density ρ_{mol}. The positions of the carbon atoms of the C_5 ring are projected onto the plane.

we examined other, nondiscontinuous, topological indicators to see if they provide a more consistent picture of the chemical bonding.

Populations of d Orbitals and Atomic Graphs. The bonding of a metal atom to the carbocyclic ring gives rise to a charge redistribution around the metal center that shows similar features in all three complexes **2**−**4**. Under the general axial symmetry of the $M(\eta^n\text{-}C_nH_n)$ unit, the metal d orbitals transform as an A representation (d_{z^2}), an E_1 representation (d_{xz}, d_{yz}), and E_2 representation ($d_{x^2-y^2}$, d_{xy}). These orbitals are potentially involved in metal-to-ring σ bonding, π bonding, and δ bonding, respectively. The d-orbital populations obtained from the experimental multipole populations[93] are given in Table 5 and clearly show that the A orbital, which is directed at the ring centroid, is the most populated, followed by the E_2 orbital. The resultant charge reorganization around the metal atom may be visualized through the deformation density (i.e., $\rho_{multipole} - \rho_{spherical}$) and the negative Laplacian isosurface plots shown in Figure 8 for complexes **2** and **4**. There are two charge concentrations directed in opposite directions along the symmetry axis of the $M(\eta^n\text{-}C_nH_n)$ unit and also charge concentrations approximately in the plane perpendicular to this axis. For complexes **2** and (not shown) **3**, there are six quite localized charge concentrations close to this plane, while for **4**, the charge concentrations merge into a continuous torus of density in the plane. This observation is easily rationalized in terms of the well-known orbital picture of bonding in metallocenes.[2] The A and E_2 orbitals barely mix with ligand-based orbitals and remain essentially pure metal d orbitals. The filled A orbital gives rise to the axial charge concentrations, while the filled E_2 set is responsible for the continuous torus of density in the plane perpendicular to the axis of symmetry. In the half-sandwich $M(CO)_3$ complexes, on the other hand, the E_2 set mixes more strongly with the carbonyl π orbitals,[21,94] and localized charge concentrations result. The charge depletions arise from the relatively low population of the destabilized E_1 set, which in the case of the metallocenes mix quite strongly with ring orbitals of the same symmetry. Because of the cylindrical symmetry, these charge depletions merge into two continuous cones. For the $M(CO)_3$ complexes **2** and **3**, on the other hand, the charge depletions are again quite localized and point in the direction of the three large charge concentrations on the three CO ligands. This is the well-known "lock and key" interaction seen in $Cr(CO)_6$, for example.[15] The atomic charges in **2**−**4**, determined from the monopole populations and from stockholder and Bader atomic-basin partitioning, are supplied in Tables S3−S5 in the Supporting Information.

The charge distribution in the valence-shell charge concentration (VSCC) of an atom is succinctly described in terms of the critical points in the negative Laplacian $-\nabla^2\rho(\mathbf{r})$, known as the atomic graph. This graph is a $[V, E, F]$ polyhedron satisfying

(93) Holladay, A.; Leung, P.; Coppens, P. *Acta Crystallogr., Sect. A* **1983**, *39*, 377.

(94) (a) Chinn, J. W., Jr.; Hall, M. B. *Organometallics* **1984**, *3*, 284. (b) Chinn, J. W., Jr.; Hall, M. B. *Inorg. Chem.* **1983**, *22*, 2759. (c) Böhm, M. C.; Gleiter, R. *J. Comput. Chem.* **1980**, *1*, 407.

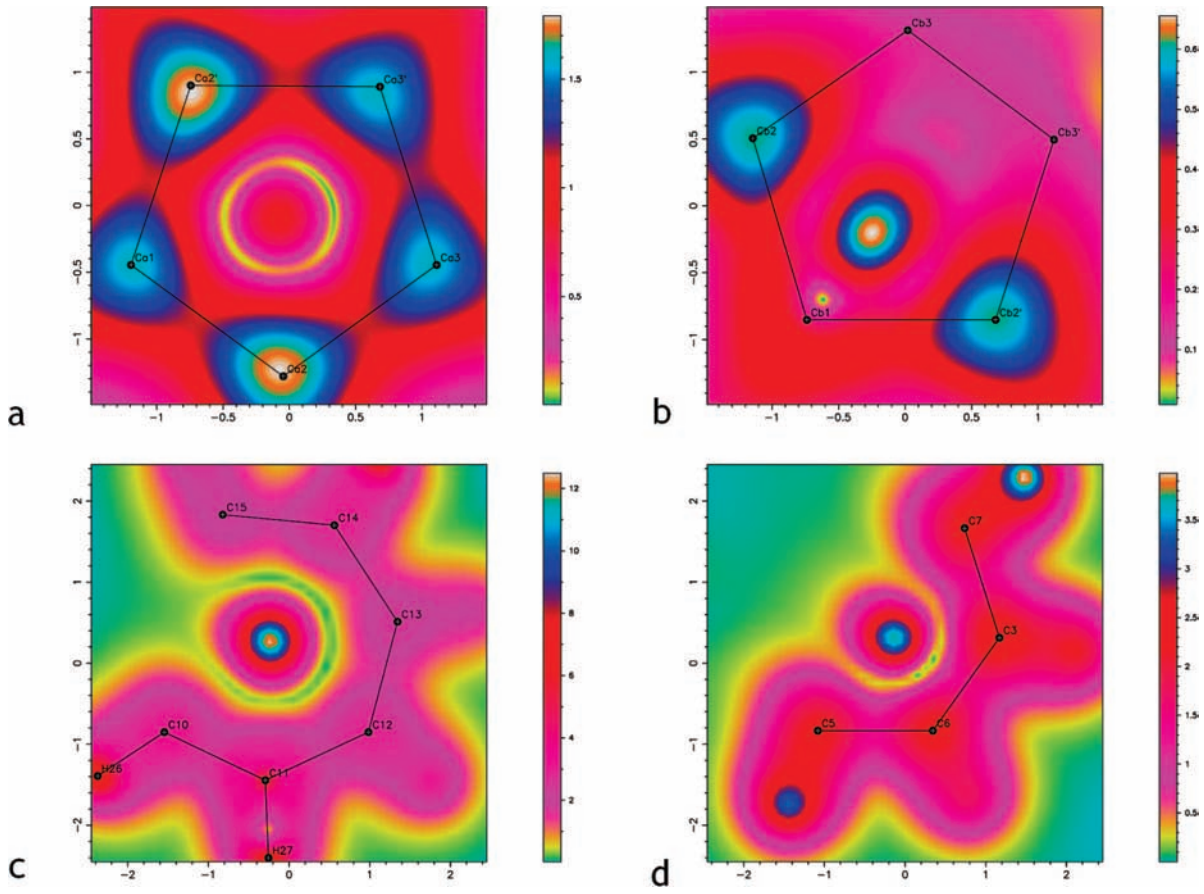

Figure 7. Plots of the magnitude of the electron density gradient $\nabla\rho(\mathbf{r})$ in the planes parallel to the coordinated ring atoms and containing the M−C bcp's for (a) ring A and (b) ring B in compound **VII** and (c) the η^6 ring and (d) the η^4 ring in compound **VIII**. The positions of the ring carbon atoms are projected onto the planes.

Table 5. Experimental d-Orbital Populations

orbital	2	3	4
z^2	1.27(1) (26.0%)	1.225(8) (32.6%)	1.84(2) (27.8%)
x^2-y^2	1.12(1) (23.0%)	0.820(8) (21.8%)	1.67(2) (25.3%)
xy	1.14(1) (23.4%)	0.822(8) (21.9%)	1.64(2) (24.8%)
xz	0.68(1) (13.9%)	0.450(8)(12.0%)	0.69(2) (10.4%)
yz	0.67(1) (13.8%)	0.441(8) (11.7%)	0.78(2) (11.8%)
total	4.89	3.75	6.61

Euler's rule $V + F - E = 2$, where V, E, and F are the numbers of vertices, edges and faces; the vertices are the (3, −3) cp's of charge concentration, the edges the saddle-point (3, −1) cp's, and the faces the (3, +1) cp's of charge depletion. The atomic graphs for the metal atoms and ring C atoms in compounds **I**−**VI** are shown in Figures S19 and S20, respectively, in the Supporting Information. Except for **VI**, the metal atomic graphs have the same underlying cuboidal [8, 12, 6] topology, which is commonly observed[15,79,95] for octahedral transition metals. As the ring size n increases, the $M(CO)_3$ cone angle decreases from 104° in **1** to 81.2° in **VI** and the six (3, −3) cp's lying off the symmetry axis become more compressed toward the plane perpendicular to this axis. In the η^8-C_8H_8 complex **VII**, these cp's become coplanar, though we were only able to identify three (3, −3) and three (3, −1) cp's in this plane.[96] The atomic graphs of the ring C atoms suggest that complexes **I** and **II** are distinct from the remainder. For **I** and **II**, a [4, 6, 4] topolology is found, which is a distorted form of the well-known tetrahedral graph for the C atom in methane.[11] For the remaining complexes, a [3, 5, 4] topology is observed, where the (3, −3) cp's are associated with the C−H and C−C covalent bonds, suggestive of sp^2 hybridization for this C atom.

Delocalization Indices. While the atomic graphs describe the distortion in the valence-shell charge distribution of the metal atom upon interaction with the ligands, they do not provide much insight into the nature of the chemical bonds formed. One such topological indicator, which does not rely on the presence of bcp's and bond paths in the charge density, is the delocalization index $\delta(\Omega_A, \Omega_B)$.[97] At the HF level, delocalization indices provide a measure of the Fermi correlation shared between atomic basins and hence of the number of electrons shared. The $\delta(\Omega_A, \Omega_B)$ indices for compounds **I**−**VI** are given in Table 6, and several trends are evident. Most obvious is the gradual reduction in the mean value of $\delta(\Omega_M, \Omega_{C(H)})$ as the ring

(95) (a) MacDougall, P. J.; Hall, M. B. *Trans. Am. Crystallogr. Assoc.* **1990**, *26*, 105. (b) Farrugia, L. J.; Evans, C. *C. R. Chim.* **2005**, *8*, 1556. (c) Abramov, Y. A.; Brammer, L.; Klooster, W. T.; Bullock, R. M. *Inorg. Chem.* **1998**, *37*, 6317. (d) Farrugia, L.; Mallinson, P. R.; Stewart, B. *Acta Crystallogr., Sect B* **2003**, *59*, 234. (e) Lee, J.-J.; Lee, G. H.; Wang, Y. *Chem.—Eur. J.* **2002**, *8*, 1821. (f) Farrugia, L. J.; Evans, C. *J. Phys. Chem. A* **2005**, *109*, 8834.

(96) Despite exhaustive searches, only three (3,−3) cp's could be located in the equatorial plane, though we suspect that there ought to be six. The algorithms for critical point searches of $-\nabla^2\rho$ in the VSCC, such as BUBBLE (Krug, P., Bader, R. F. W., Department of Chemistry, McMaster University, Hamilton, ON, 1990) are not ideally suited for locating many points in a plane.

(97) (a) Fradera, X.; Austen, M. A.; Bader, R. F. W. *J. Phys Chem. A* **1999**, *103*, 304. (b) Ángyán, J. G.; Loos, M.; Mayer, I. *J. Phys. Chem.* **1994**, *98*, 5244.

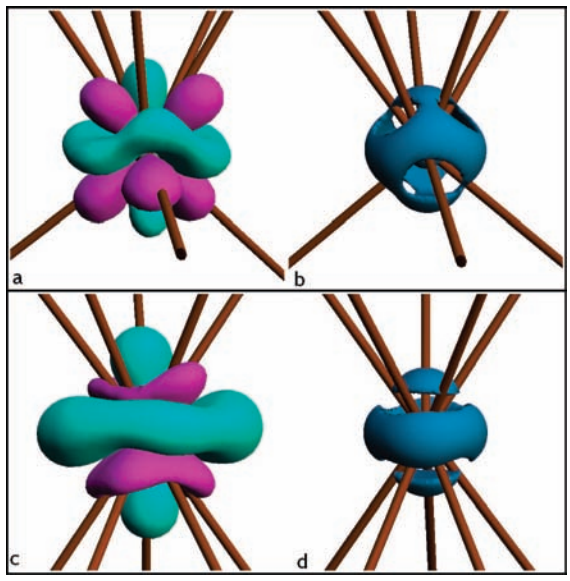

Figure 8. Isosurface plots of (left) the experimental deformation density and (right) the negative Laplacian for the metal atoms in (a, b) (η^5-C_5H_5)Mn(CO)$_3$ (**2**) and (c, d) (*E*)-{(η^5-C_5H_4)CF=CF(η^5-C_5H_4)}(η^5-C_5H_5)$_2$Fe$_2$ (**4**). Deformation density levels are set at (cyan) +0.5 and (magenta) −0.5 e Å^{-3} and the negative Laplacian level at 500 e Å^{-5}.

Table 6. Delocalization Indices $\delta(\Omega_A, \Omega_B)$ in Compounds **I**−**VI**

A, B	I	II	III	IV	V	VI
M, C(O)	1.01	1.08	1.13	1.04	0.79	0.60
M, O	0.16	0.18	0.20	0.19	0.14	0.11
M, C(H)	0.65	0.54	0.34	0.30	0.32	0.23
M, H	0.03	0.02	0.01	0.01	0.01	0.01
C, C	1.16	1.14	1.25	1.28	1.27	1.31
C, H	0.94	0.96	0.96	0.95	0.95	0.94
C, O	1.63	1.60	1.57	1.57	1.61	1.66
$\sum\delta$(M−ring)[a]	2.05	2.23	1.77	1.86	2.32	1.89

[a] Defined as $\sum_{i=1}^{n}[\delta(\Omega_{M_i}, \Omega_{C_i(H)}) + \delta(\Omega_{M_i}, \Omega_{H_i})]$.

size increases. This is correlated with the increase in the M−C(H) bond length (Figure S16 in the Supporting Information), but it is interesting to note that the sum of all of the delocalization indices involving the metal atom and the ring C and H atoms, $\sum\delta$(M−ring), is roughly constant at ∼2. While there is no clear physical interpretation of $\delta(\Omega_A, \Omega_B)$ values computed from a DFT wave function, it has been observed[70] that their magnitudes are very similar to those calculated at the HF level. Thus, we may assume that a similar number of electrons, approximately four, are involved in the metal−ring bonding, regardless of the ring size. The variation in individual $\delta(\Omega_M, \Omega_{C(H)})$ values for a particular complex is small, which implies roughly equal chemical bonding for all M−C_{ring} interactions. Moreover, the formal hapticity of the rings in complexes **VII** and **VIII** is unambiguously reflected in the indices $\delta(\Omega_M, \Omega_C)$, which are very small for the formally nonbonded M−C interactions (see Table 7). These results are of course consistent with chemical sense and the virial graphs but not necessarily with the molecular graphs. The $\delta(\Omega_C, \Omega_C)$ indices also show a correlation with the C−C distances (Figure S18 in the Supporting Information), apart from the outlier of complex **I**, while the $\delta(\Omega_C, \Omega_H)$ and $\delta(\Omega_C, \Omega_O)$ indices are reasonably constant across the series.

Source Function. The computation of the delocalization index requires the first- and second-order density matrices, which are not generally available for experimentally determined densities.

Table 7. Delocalization Indices $\delta(\Omega_M, \Omega_C)$ in Compounds **VII** and **VIII**

VII

	C1	C2	C3
ring A	0.34	0.36	0.25
ring B	0.34	0.34	0.08

VIII

	C10	C11[a]	C12	C13	C14[a]	C15	C16	C2
η^6 ring	0.56	0.45	0.38	0.38	0.41	0.51	0.04	0.04
	C5	C6[a]	C3	C7	C8	C9	C17	C4
η^4 ring	0.53	0.52	0.47	0.45	0.08	0.07	0.07	0.09

[a] Atom is associated with a bond path.

It has been shown by Bader and Gatti[98] that the electron density at any point **r** within a molecule may be viewed as consisting of contributions from a source operating at all other points **r′**. The local source (LS) contribution at reference position **r** from points **r′** is then given by

$$\mathrm{LS}(\mathbf{r}, \mathbf{r}') = -\frac{1}{4\pi}\int \frac{\nabla^2\rho(\mathbf{r}')}{|\mathbf{r}-\mathbf{r}'|}\,\mathrm{d}\mathbf{r}'$$

Integration over the regions of space bounded by the zero-flux surfaces affords the atomic contribution $S(\mathbf{r}, \Omega)$ to the density at **r**, and the total density $\rho(\mathbf{r})$ is then the sum of all of the atomic contributions:

$$\rho(\mathbf{r}) = \sum\nolimits_{\Omega}\int_{\Omega}\mathrm{LS}(\mathbf{r}, \mathbf{r}')\,\mathrm{d}\mathbf{r}' \equiv \sum\nolimits_{\Omega} S(\mathbf{r}, \Omega)$$

The integrated form of the source function (SF) provides a measure of the relative importance of each atomic basin's contribution to the density at the reference point (rp). Since the SF depends only on the derivative $\nabla^2\rho(\mathbf{r})$, it may be obtained from experimental densities without approximation and thus provides an experimental method for determining nonlocal contributions to $\rho(\mathbf{r})$. Gatti et al.[99a] have proposed that the SF provides pertinent chemical information. It is normal to use as rp's the critical points in $\rho(\mathbf{r})$, as these provide the least biased positions for information on chemical bonding, though of course any point would be valid. The SF has been used to investigate several disparate types of chemical interactions, including weak and strong hydrogen bonds,[99] organometallic metal−metal bonds,[32,100,101] transition-metal σ-silane complexes,[102] and the iron−ligand interactions in Fe{$C(CH_2)_3$}$(CO)_3$.[33] These studies have relied mainly on the SFs obtained from theoretical densities, but there are recent reports[32,101,102] involving SFs from experimental densities.

Figure 9 shows the integrated SF contributions for complex **2** obtained from theory, while corresponding experimental and

(98) Bader, R. F. W.; Gatti, C. *Chem. Phys. Lett.* **1998**, *287*, 233.
(99) (a) Gatti, C.; Cargnoni, F.; Bertini, L. *J. Comput. Chem.* **2003**, *24*, 422. (b) Overgaard, J.; Schiott, B.; Larsen, F. K.; Iversen, B. B. *Chem.—Eur. J.* **2001**, *7*, 3756. (c) Sørensen, J.; Clausen, H. F.; Poulsen, R. D.; Overgaard, J.; Schiott, B. *J. Phys. Chem. A* **2007**, *111*, 345.
(100) Gatti, C.; Lasi, D. *Faraday Discuss.* **2007**, *135*, 55.
(101) Overgaard, J.; Clausen, H. F.; Platts, J. A.; Iversen, B. B. *J. Am. Chem. Soc.* **2008**, *130*, 3834.
(102) McGrady, G. S.; Sirsch, P.; Chatterton, N. P.; Ostermann, A.; Gatti, C.; Altmannshofer, S.; Herz, V.; Eickerling, G.; Scherer, W. 2008, arXiv:0811:110451v1. arXiv.org e-Print archive. http://arxiv.org/abs/0811.0451v1 (accessed Dec 12, 2008).

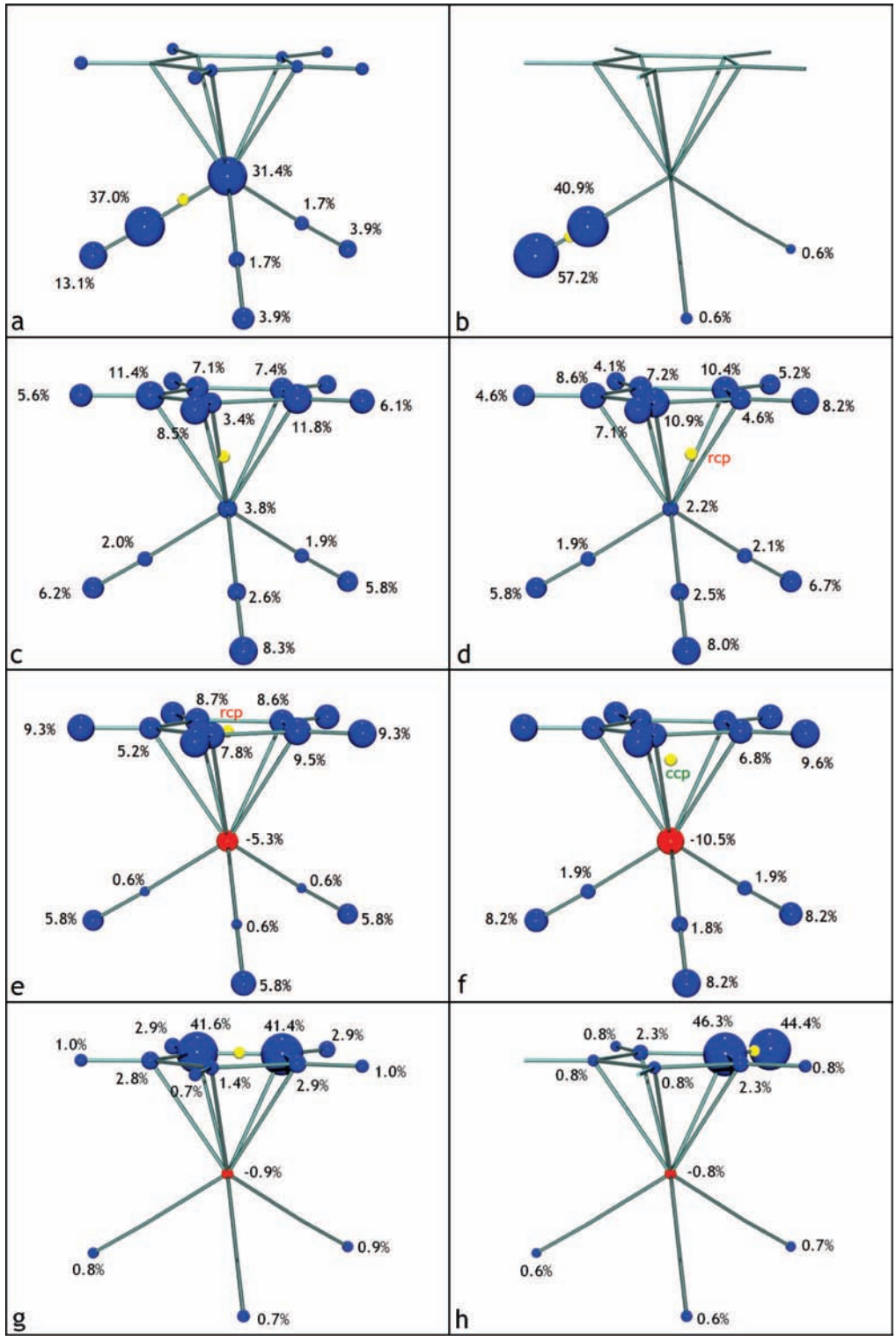

Figure 9. Theoretical integrated source function in complex **2**, with the reference points located at (a) the Mn−C(O) bcp (92.8%), (b) the C−O bcp (99.2%), (c) the Mn−C(Cp) bcp (30.5%), (d) the Mn−C(Cp) rcp (29.2%), (e) the C_5 rcp (13.9%) (f) the C_5 ccp (19.8%), (g) the C−C bcp (1.5%), and (h) the C−H bcp (0.6%) (values in parentheses are the % contributions from the $Mn(CO)_3$ group). The volume of the spheres on the atomic centers are proportional to the percentage contributions from the atomic basins; positive contributions (sources) are shown as blue spheres and negative contributions (sinks) as red spheres. The reference points are shown as yellow spheres, and absolute source contributions less than 0.5% are not shown.

theoretical plots for **2** and **3** are given in the Supporting Information. It is clear that at least in a qualitative sense, there is excellent agreement between theory and experiment. When the rp is at the Mn−C(O) bcp, nearly 70% of the density is recovered from the basins of the Mn and C atoms, while a significant contribution also comes from the basin of the carbonyl O atom. This latter contribution cannot be simply interpreted as a signal of Mn−CO π back-bonding. We have previously shown[33] that the C and O basins' percentage source contributions at the B−C bcp in the adduct H_3B←CO are very

similar, and in that case, no B−C π back-bonding is possible. There is also a small but detectable (∼7%) delocalization onto the Cp ring. However, when the rp is at the C−O bcp, the extent of SF contributions from these two atomic basins alone is more than 98%, and there is an insignificant contribution from the Cp ring. This SF distribution is typical of the transition-metal−carbonyl bonds described so far.[33,100] In fact, in all of the reported systems, the SF contributions from the O and C basins to the C−O bcp are remarkably constant at ∼58 and 40%, respectively, indicative of the high degree of transferability of the carbonyl group.

When the rp is located at the C−C or C−H bcp in the cyclopentadienyl ligand (Figure 9g,h), there is again superb agreement between theory and experiment. The degrees of localization from the two basins directly involved in the bond are ∼83 and 90%, respectively, and there is only a very tiny contribution from the $Mn(CO)_3$ group. In view of the delocalization of π density in these conjugated rings, this result may seem surprising. The greatest numerical differences in the SF between theory and experiment come when the rp is placed between the ring and the Mn atom. The contribution of the Mn basin is always greater in the experimental SF, so it never acts as a sink. Nevertheless, the qualitative features remain essentially the same. Thus, there are only small differences in the relative contributions of all of the basins when the rp is at a bcp or an rcp in the [5, 5] ring of cp's (see Figure 9c,d). It is immediately obvious that regardless of the exact placement of the rp in this zone, there are significant contributions from all of the C and H basins of the ring. This may be taken as an indicator of the delocalized nature of the Mn−ring interaction. It is very important to note that the SF for the Mn−C interaction that is missing as a bond path in the experimental density is essentially identical to all the others. The global contribution of the $Mn(CO)_3$ group is ∼30% in the theoretical SF and slightly more (∼33%) in the experimental SF, regardless of the exact placement of the rp in the [5, 5] ring plane.

The features in the SF distributions for the metal−ring interactions in complexes **3** and **4** are essentially identical to those discussed above for **2**. The SF distributions for complexes **I**, **II**, **V**, and **VI**, which are given in the Supporting Information, also display the same general features. Interestingly, the SF for **4** does not provide much evidence for delocalization between the two ferrocene units. When the rp is located at the alkenyl C═C bcp (Figure 10a), the SF is highly localized onto the two C basins (∼85%), with a further 8% provided by the two F basins; however, when the rp is at the Fe−C10 bcp (Figure 10e), there is a small delocalization into the alkenyl unit. The CH···F interaction in **4** provides an interesting case, with a characteristic and highly delocalized SF (Figure 10h). The three interacting atomic basins themselves act as very large sinks (−61.8% in total), while the remaining F basin provides the single largest source (26.4%). When a basin acts as a sink, the kinetic energy density dominates over the potential energy density when averaged over that basin. It should be noted that since the electron density at the bcp is only 0.069 e $Å^{-3}$, the percentage error (3.8%) in the source-recovered density is quite high, so integration errors render the source reconstruction qualitative at best.[103] Nevertheless, it is clear that this SF distribution is quite different in character from ones discussed previously. In particular, even basins that are quite distant from the rp provide significant contributions. Similar features are observed in the case of weak H bonds,[99] and we have recently observed the same in Cu(II) 3-aminopropanolato complexes.[104] We take this as a signal that the CH···F interaction has little covalency and is essentially electrostatic in nature.

The SF is also useful as a discriminator of the formal hapticities in complexes **VII** and **VIII** (Figures S30−S32 in the Supporting Information). When the rp is located at a general point in space for which there is no evidence for significant chemical interactions (e.g., the midpoint of the C−H···H−C vector or the C−H···O vector), the SF distributions (Figure S30g,h) are very similar to that observed for the CH···F interaction in **4**. Our interpretation is that the relatively low electron density at these rp's is not dominated by any charge buildup from local covalent chemical interactions but rather determined through the long-range electrostatic pressure exerted by the other atomic basins. This results in a very delocalized SF distribution. A similar SF distribution is seen when the rp is located at the midpoint of the Cr−C(B3) vector (Figure S30a), which is formally a nonbonded interaction. On the other hand, for the Cr−C(B2) and Cr−C(B1) interactions (Figure S30b,c), the SF distribution more closely resembles that observed for the metal−C_{ring} interactions in **2**−**4**. A clear distinction is thus seen in the SF for the formally bonded and nonbonded Cr−C interactions for the η^3-C_5H_5 ring. This also applies to the formal η^5-C_5H_5 ring (Figure S30d−f), where all of the Cr−C_{ring} SF distributions resemble those seen for complexes **2**−**4**. For complex **VIII**, the situation is similar, though perhaps a little less clear-cut. When the rp is associated with the *inner* C atoms of the η^4-C_8H_8 or η^6-C_8H_8 rings, the SF distribution is very similar to that seen for the closed rings in complexes **I**−**VI**, with a delocalized SF where all of the basins act as sources. When associated with the long, formally nonbonded Fe−C vectors, on the other hand, the SF resembles that seen for the CH···F interaction in **4**, with a number of basins acting as sinks. The situation is intermediate for those C atoms at the ends of the conjugated chains.

Conclusions

The interaction of a transition metal with a closed or open π-hydrocarbyl ligand generates a zone of very flat ρ and very low $\nabla\rho$ in which any M−C bond critical points must be located. This almost inevitably leads to a M−C_{ring} topology that is close to a catastrophe situation, and as a result, the number of bond paths cannot be predicted with any certainty. In such circumstances, a localized description of the chemical bonding in terms of the individual M−C_{ring} bond paths is not completely satisfactory. Continuous QTAIM indicators, which do not rely on the presence of a bcp, such as the delocalization indices and the source function, provide a picture of the chemical interactions that is more in line with chemical experience. We may

(103) The relative accuracy of the reconstruction of $\rho(\mathbf{r})$ from the summation of atomic sources may be gauged by the quantity ER($\mathbf{r}$), defined as follows:[99]

$$\mathrm{ER}(\mathbf{r}) = \frac{|\rho(\mathbf{r}) - \sum_{\Omega} S(\mathbf{r}, \Omega)|}{\rho(\mathbf{r})} \times 100\%$$

ER($\mathbf{r}$) is typically ∼1% or less for strong covalent interactions, where $\rho(\mathbf{r}_{bcp}) \geq 0.2$ e $Å.^{-3}$ Much higher values of ER($\mathbf{r}$) are observed for those reference points with very small values of $\rho(\mathbf{r})$ because of the higher percentage errors incurred in reconstructing $\rho(\mathbf{r})$ through the SF summation.

(104) Farrugia, L. J.; Middlemiss, D. S.; Sillanpää, R.; Seppälä, P. *J. Phys. Chem. A* **2008**, *112*, 9050.

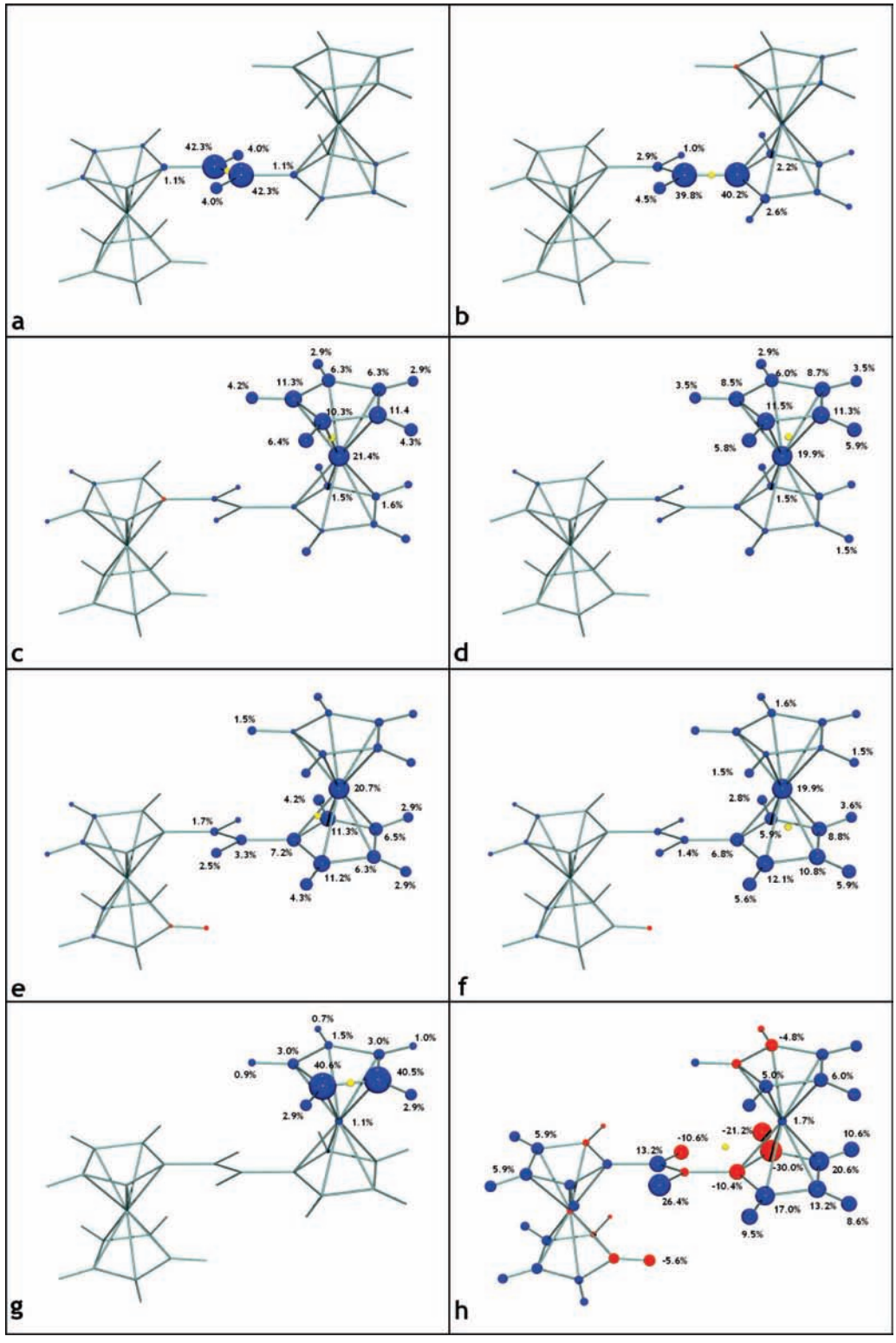

Figure 10. Theoretical integrated source function in complex **4**, with the reference points located at (a) the C═C bcp, (b) the C−C(Cp) bcp, (c) the Fe−C(Cp-top) bcp, (d) the Fe−C(Cp-top) rcp, (e) the Fe−C(Cp-bottom) bcp, (f) the Fe−C(Cp-bottom) rcp,(g) the Cp C−C bcp, and (h) the CH···F bcp. Other details are the same as in Figure 9.

regard these systems as having a very soft potential energy surface for the metal−π-hydrocarbyl interaction. Slightly different density models (either experimental or theoretical) effectively explore this surface and may give rise to differing numbers of M−C_{ring} bond paths. Since the M−C_{ring} topology is in a chaotic situation, it is clear that any search for underlying causes of "missing" bond paths in terms of the experimental data quality, refinement procedures, or multipole models, etc., is likely to be a futile one. To emphasize this concern, we note

(105) Sparkes, H. A.; Brayshaw, S. K.; Weller, A. S.; Howard, J. A. K. *Acta Crystallogr., Sect. B* **2008**, *64*, 550.

that two cases of "missing" bond paths for metal−π-hydrocarbyl complexes have recently been presented and discussed in some detail.[101,105]

Acknowledgment. This work was supported by the University of Glasgow and the EPSRC under Grant GR/M91433 for the purchase of a KappaCCD diffractometer. The New Zealand Foundation for Research, Science & Technology is thanked for financial support (PDRA) for C.E.

Supporting Information Available: Final refined parameters and observed and calculated structure factors for the multipole refinements (CIF); Figures S1−S34 and Tables S1−S6; and complete ref 65. This material is available free of charge via the Internet at http://pubs.acs.org.

JA808303J